Microneurography as a Minimally Invasive Method to Assess Target Engagement During Neuromodulation

Nishant Verma[1,2], Bruce Knudsen[1,2], Aaron Gholston[2], Aaron Skubal[1,2], Megan Settell[1,2], James Trevathan[1,2], Stephan Blanz[1,2], Jennifer Frank[1], Kip Ludwig[1,2,3]

[1]Department of Biomedical Engineering, University of Wisconsin – Madison, Madison, WI, USA
[2]Wisconsin Institute for Translational Neuroengineering (WITNe) – Madison, Madison, WI, USA
[3]Department of Neurosurgery, University of Wisconsin – Madison, Madison, WI, USA

Abstract

Objective. Peripheral neural signals recorded during neuromodulation therapies provide insights into local neural target engagement and serve as a sensitive biomarker of physiological effect. Although these applications make peripheral recordings important for furthering neuromodulation therapies, the invasive nature of conventional nerve cuffs and longitudinal intrafascicular electrodes (LIFE) limit their clinical utility. Furthermore, cuff electrodes typically record clear asynchronous neural activity in small animal models but not in human-scaled models. Microneurography, a minimally invasive technique, is already used routinely in humans to record asynchronous neural activity in the periphery. However, the relative performance of microneurography microelectrodes, compared to cuff and LIFE electrodes, in measuring neural signals relevant to neuromodulation therapies is not well understood.

Approach. To address this gap, we performed cervical vagus nerve evoked compound action potential (ECAP) and spontaneous activity recordings in a human-scaled large animal model – the pig. Additionally, we recorded sensory evoked activity and both invasively and non-invasively evoked CAPs from the great auricular nerve (GAN). In aggregate, this study assesses the potential of microneurography microelectrodes to measure neural activity during neuromodulation therapies with statistically powered and pre-registered outcomes (https://osf.io/y9k6j).

Main results. The cuff recorded the largest ECAP signal ($p<0.01$) and had the lowest noise floor amongst the evaluated electrodes. Despite the lower signal to noise ratio, microneurography microelectrodes were able to detect the threshold for neural activation with similar sensitivity to cuff and LIFE electrodes once a dose-response curve was constructed. Furthermore, the microneurography microelectrode was the only electrode to record distinct sensory evoked neural activity ($p<0.01$).

Significance. The results suggest that microneurography microelectrodes could enable minimally invasive assessment of neural activity for individual subjects. This will further neuromodulation therapies by providing a real-time biomarker to adjust electrode placement and stimulation parameters to optimize the on- to off-target neural fiber engagement and study mechanisms of action.

Introduction

Inconsistent local neural target engagement and poor isolation of on- and off-target neural substrates is critically limiting neuromodulation therapies (Heusser et al., 2016; De Ferrari et al., 2017; Verma et al., 2021a). Direct measurements of neural activity during the acute deployment of neuromodulation therapies could 1) guide electrode design and placement to chronically improve consistency of local target engagement and 2) prove critical for understanding on- and off-target neural substrates and therapeutic mechanisms of action (Verma et al., 2021a).

Although these applications make it pertinent to acutely record neural activity from the peripheral nervous system, the invasiveness of conventional cuffs and longitudinal intrafascicular electrodes (LIFE) electrodes limit their clinical utility. In contrast, clinical microneurography microelectrodes are minimally invasively placed into a nerve using ultrasound guidance or palpation but have yet to be explored for understanding neuromodulation therapies. Microneurography microelectrodes are often made of tungsten and have a smaller recording tip compared to cuff and LIFE electrodes and do not require a surgical window for placement. Microneurography microelectrodes are already used in humans to perform acute recordings for diagnostic and research purposes (Macefield, 2020), but have yet to be evaluated for informing neuromodulation therapies. The relative performance of microneurography microelectrodes, compared to conventional cuffs and LIFE electrodes, in measuring neural signals relevant to neuromodulation therapies is also not well understood.

To understand the relative performance of microneurography microelectrodes compared to conventional cuff and intrafascicular electrodes, we performed a side-by-side comparison of recording electrode styles for the peripheral nervous system in a human-scaled model (Fig. 1A). We compared each electrode's ability to measure both synchronous electrically evoked compound action potentials (ECAPs) (Fig. 1B, top) and asynchronous sensory evoked and spontaneously occurring activity (Fig. 1B, bottom). ECAPs represent the recruitment of neurons around the stimulation electrode and are a direct measurement of local on- and off-target neural engagement. Spontaneously occurring activity is a real-time and sensitive measure of changes induced by neurostimulation, sometimes even before physiological changes become evident (Gonzalez-Gonzalez et al., 2021; Chao et al., 2021). Growing interest in modulating spontaneously occurring neural activity outside the period of stimulation (e.g., burst stimulation for chronic pain therapy) will make spontaneously occurring activity a key biomarker in neuromodulation therapies.

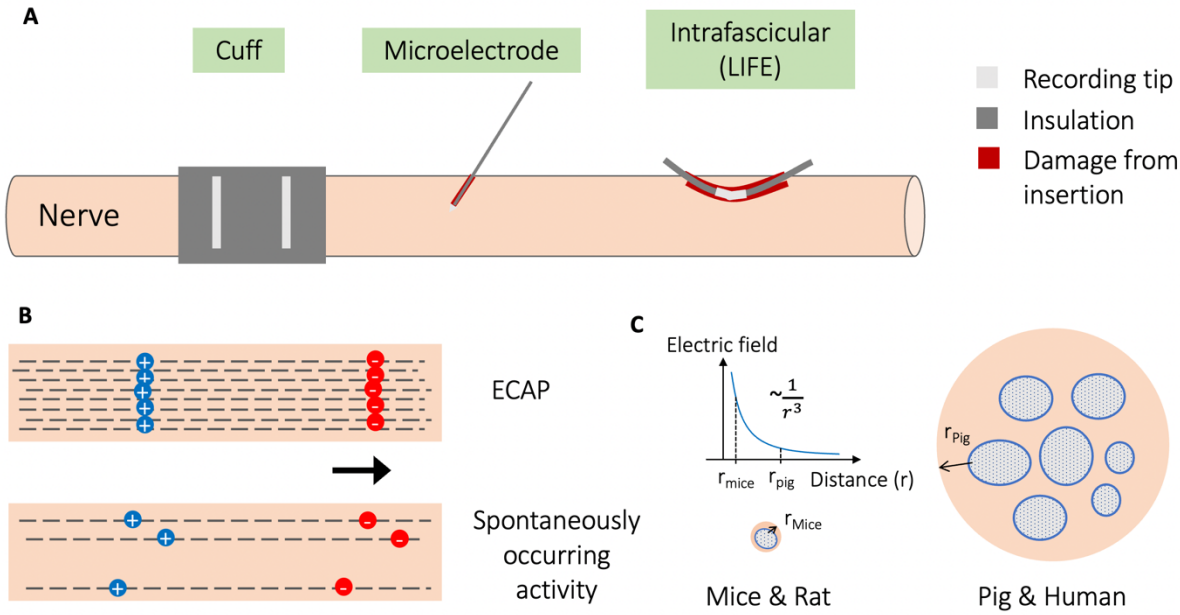

Figure 1: Concept of ECAP vs. spontaneously occurring neural activity and relevance of scale.
(A) Illustration showing the three different types of recording electrodes being characterized for their performance in measuring neural signals from the peripheral nervous system. The LIFE has the larger recording tip between the two penetrating electrodes and causes more damage to tissue upon insertion, indicated by the red blood track.
(B) ECAP vs. spontaneously occurring neural activity illustrated by number of fibers activated and synchrony of neural activity. Both illustrate a neural signal as a moving dipole with a finite wavelength that increases with conduction velocity and fiber size.
(C) Cartoon illustrating the relevance of scale in interpreting neural recording electrode performance. For example, in the cervical vagus nerve for smaller mammals, there is 1) less distance between the neural fiber and the surface of the nerve, where a recording electrode is placed, and hence less fall of in electric field 2) there is a thinner layer of perineurium insulation, and hence less fall of in electric field and 3) there are fewer and smaller fascicles compared to a larger mammal.

We performed the experiments in pigs, a human-scaled model, which is critical for the translatability of the findings (Koh et al., 2022). Studies in animal models with smaller peripheral nerves, such as rodents, have shown recordings of spontaneously occurring neural activity made with non-penetrating hook and cuff electrodes (Moncrief and Kaufman, 2006; Silverman et al., 2018; Stumpp et al., 2020). However, this might not be possible in human-scaled nerves, due to their larger diameter and multi fascicular make up (Settell et al., 2020; Koh et al., 2022). Specifically, the vagus nerve in mice and rat are 200-300 μm in diameter with a single fascicle while the vagus nerve in humans and pigs are 2-3 mm in diameter and consist of many fascicles (Settell et al., 2020). The larger diameter of the nerve and thicker perineurium and epineurium increases the distance between the firing neuron and the recording electrode, thereby reducing the recorded signal amplitude (Yoo et al., 2013) (Fig. 1C). Furthermore, the multi fascicular make-up of human nerves, with bundles of neurons wrapped in low electrical

conductivity perineurium, also reduces the available signal magnitude at the surface of the nerve. As an example, Yoo and colleagues (2013) reported they had to de-sheath the epineurium of vagus nerve in dogs, thereby reducing nerve diameter and epineurium electrical impedance, to clearly record C-fiber ECAP components. The increased distance from neurons to the surface of the nerve and the multi-fascicular make-up of the nerve makes it challenging to record neural activity with non-penetrating electrodes in human-scaled models.

Here, we evaluated microneurography microelectrodes against cuff and LIFE electrodes in their ability to measure invasively and non-invasively evoked CAPs, sensory evoked neural activity, and spontaneously occurring activity in the peripheral nerves of swine, a large animal model representative of the human peripheral nervous system (Settell et al., 2020). The cervical vagus, a major autonomic nerve of great interest as a neuromodulation therapy target (Johnson and Wilson, 2018), was used as the first model nerve. In addition, the great auricular nerve (GAN), a sensory nerve innervating the ear and implicated in auricular vagus nerve stimulation (aVNS) (Verma at el., 2021a), was used as the second model nerve to evaluate sensory evoked potential and non-invasively evoked CAP recordings. Judicious choice of reference electrode placement is known to optimize neural signal fidelity and minimize artifact and were explored and discussed here. Furthermore, common non-neural artifacts in electrophysiology recordings were noted along with discussion on appropriate controls to verify neural recording authenticity. Based on the findings, we summarize considerations and recommend minimally invasive microneurography as a technique that can be used acutely during the deployment of neuromodulation therapies to inform electrode placement, electrode design, and selection of stimulation parameters and to investigate therapeutic mechanisms of action.

Methods

In this study, we characterized cuff electrodes, longitudinal intrafascicular electrodes (LIFE), an intrafascicular electrode used in pre-clinical studies (Yoshida and Stein, 1999; Nicolai et al., 2020), and microneurography microelectrodes, a clinical microelectrode used routinely in humans (Macefield, 2021), in their ability to measure neural activity in the peripheral nervous system. The cervical vagus, a major autonomic nerve innervating organs in the thorax and abdomen as well as muscles in the throat, and the great auricular nerve (GAN), a sensory nerve innervating the ear and periauricular region, were used as model nerves due to their relevance in existing peripheral neuromodulation therapies – invasive vagus nerve stimulators for epilepsy and depression (Johnson and Wilson, 2018) and non-invasive aVNS (Verma et al., 2021a), respectively.

Pre-registration

Pilot experiments (n=10) were conducted to refine the surgery and establish the study protocol. The study was then pre-registered (https://osf.io/y9k6j) with sequentially defined primary, secondary, and exploratory outcomes, statistical comparisons, analysis parameters, and sample size (n=6). The confirmatory experiments were conducted after pre-registration with no exclusion of subjects.

Recording electrodes

Photographs of the recording electrodes are in Supplementary Material. The microneurography microelectrodes were fabricated of tungsten with an impedance of 0.8-1.2 MΩ at 1 kHz, shaft diameter of 250 μm and rounded tip diameter of ~5 μm (estimate), part number UNA40GCT (FHC Inc., ME, USA). The vagus recording cuff was fabricated of platinum and silicone with three cylindrical contacts 1 mm in width, separated by 3 mm from each other, and 2 mm from the edge of the silicone. The three cylindrical contacts themselves were split into seven contacts each (1 x 1 mm size) with all seven contacts electrically connected – giving the cuff improved mechanical flexibility. The vagus recording cuff had an inner diameter of 3 mm (Ardiem Medical Inc., PA, USA). The LIFEs were fabricated in house of platinum iridium wire with 0.004” diameter with insulation and an exposed window length of ~2 mm and diameter of 0.002”. The impedance of the LIFEs were 1-10 kΩ at 1 kHz. The GAN recording cuffs were identical to the GAN stimulation cuffs and were fabricated in house of two platinum wires (0.005" diameter), separated by ~1 mm, glued (using a silicone-based glue) into a split silicone tube of 0.75 mm inner diameter with a total length of 3 mm (Fig. 2B).

Acute swine experiments

An equal number of male and female domestic swine of weight 50-60 kg (age ~3 months) were used in the (n=6) confirmatory experiments. All animal care and procedures were approved by the University of Wisconsin – Madison Institutional Animal Care and Use Committee (IACUC).

Anesthesia

An intramuscular injection of Telazol (6 mg/kg) and Xylazine (2 mg/kg) was used to induce anesthesia. The animals were ventilated, and the surgical anesthetic plane was maintained with inhaled Isoflurane (1-2%) and intravenous Fentanyl (12-30 mcg/kg/hr) administered with lactated Ringer’s solution (LRS) for analgesia.

Several hours into the experiment, an onset of tremoring was observed in the animals. Pigs are known to be especially prone to tremoring during anesthesia (Ringer et al., 2016). The tremoring was observed despite confirmation of the surgical anesthetic plane by means of nasal septum pinch, jaw slackness, unresponsiveness to corneal reflex, and verification of other

physiologic parameters such as temperature, blood glucose, and blood pH. The tremoring persisted despite increased dosing of Isoflurane and Fentanyl. We found either intramuscular injection of Telazol (4-6 mg/kg) or intravenous Ketamine (10 mg/kg/hr) eliminated the tremoring. The effects of Telazol lasted for ~2 hours while Ketamine effects on tremoring washed in and out in ~15 minutes.

A muscle paralytic, vecuronium, was administered intravenously during vagus nerve recordings to abate recording artifacts resulting from myogenic electric field spillover due to electrically evoked muscle movement (Yoo et al., 2013; Nicolai et al., 2020; Blanz et al., 2022) or ongoing tremoring – without cardiac blunting effects. We delivered vecuronium as a 0.1 mg/kg bolus over 1 minute followed by 1-1.5 mg/kg/hr constant rate infusion.

Physiological recording

Heart rate from a pulse transducer (AD Instruments, Sydney, Australia) and EKG (AD Instruments, Sydney, Australia), blood pressure from a femoral artery catheter (Millar, Houston, TX, USA), temperature from a rectal probe (Physitemp, Clifton, NJ, USA), and SpO2 from a pulse oximeter (Nonin, Plymouth, MN, USA) applied on the tongue were recorded through the PowerLabs 8/35 (AD Instruments, Sydney, Australia). Stimulation timings were synced with the physiological recording for further analysis of stimulation-evoked physiological changes. Stimulation-evoked heart rate changes were calculated as the difference between the mean heart rate 1-3 s before stimulation and the maximum change in heart rate during stimulation (Blanz et al., 2022).

Cervical vagus nerve preparation and electrophysiology

ECAPs from invasive stimulation and spontaneous activity were measured from the cervical vagus nerve (Fig. 2A, C). With the subject in a supine position, a midline approach was used to access the left carotid sheath. The carotid artery was mobilized and carefully retracted to minimize obstruction to blood flow. The cervical vagus nerve was exposed for a length of 9-12 cm and instrumented with a bipolar stimulation electrode (Fig. 2A: 2 mm diameter circular contacts) caudal to the superior laryngeal branching off the nodose ganglion (Settell et al., 2020). Three replicates of the LIFE and microneurography microelectrodes and a cuff electrode with three recording contacts were instrumented on the nerve caudal to the stimulation electrode. A separation of >4 cm was kept between the stimulation electrode and the closest recording electrode. The order of the recording electrodes (cuff, intrafascicular, and microneurography microelectrode) were pseudo-randomized per subject to reduce bias arising from distance between the stimulation and recording electrode, which is known to affect ECAP morphology (Parker et al., 2020). A reference electrode, similar in design to the recording LIFE electrodes, inserted in superficial fat was used to reference the cuff and LIFE electrodes while a

microneurography microelectrode inserted in superficial fat was used to reference the microneurography microelectrodes. Superficial fat was selected as it has the closest material to the fatty tissue of nerves and best matches the mechanical and electrochemical environment of the recording electrodes. An off-nerve reference also allowed for post-hoc virtual re-referencing between all recording electrode pairs for each recording modality. The reference electrode site was selected at a distance approximately equidistant from the stimulation electrode to the recording electrodes to match the representation of the stimulation artifact. Additional recordings were collected with various on-nerve references.

A Tucker-Davis Technologies (TDT) electrophysiology system was used for stimulation and recording. The analog front-end and digitizer were on the battery-powered Subject Interface Module (SIM, TDT Inc., FL, USA). Data was collected at 25 kHz and digitized with a 28-bit Sigma-Delta (45% low-pass anti-aliasing filter) analog to digital converter (ADC) without amplification. High impedance (microneurography microelectrodes) and low impedance (LIFEs and cuff) were recorded into two separate recording cards with an active (ZC32, TDT Inc., FL, USA) and passive (S-Box, TDT Inc., FL, USA) head stage respectively. Stimulation was delivered in bipolar mode with two floating current sources.

ECAPs were recorded during delivery of 750 biphasic stimulation pulses with a 200 μs pulse width at 25 Hz with stimulation amplitudes between 0 and 10 mA presented in a randomized order. Time locked recordings were made through the recording electrodes.

Great auricular nerve preparation and electrophysiology

The great auricular nerve (GAN) innervates the auricle and is implicated as an off-target nerve in aVNS therapies. The GAN is also purported to be part of the therapeutic effect pathway for auricular stimulation-based therapies addressing Parkinson's disease (Cakmak et al., 2017) and pain (Kaniusas et al., 2019). Therefore, measuring neural activity directly from the GAN can be used to assess both on- and off-target neural activation for auricular stimulation to inform stimulation electrode location and parameters. The GAN (Fig. 2C, top) is also morphologically distinct from the cervical vagus nerve (Fig. 2D, bottom), which is larger and contains more fascicles. Characterizing recording electrode performance in both these nerves improves the applicability of the results. The GAN was also selected because it was more surgically accessible than the auricular branch of the vagus (ABVN), and potentially amenable to percutaneous microneurography under ultrasound, which may be problematic for the ABVN due to its anatomical course. ECAPs from invasive stimulation and non-invasive stimulation and sensory evoked neural activity in response to sensory stroking were measured from the GAN. The GAN was accessed by the following approach, which to our knowledge, is the first surgical description of a procedure specifically accessing and identifying the GAN in swine.

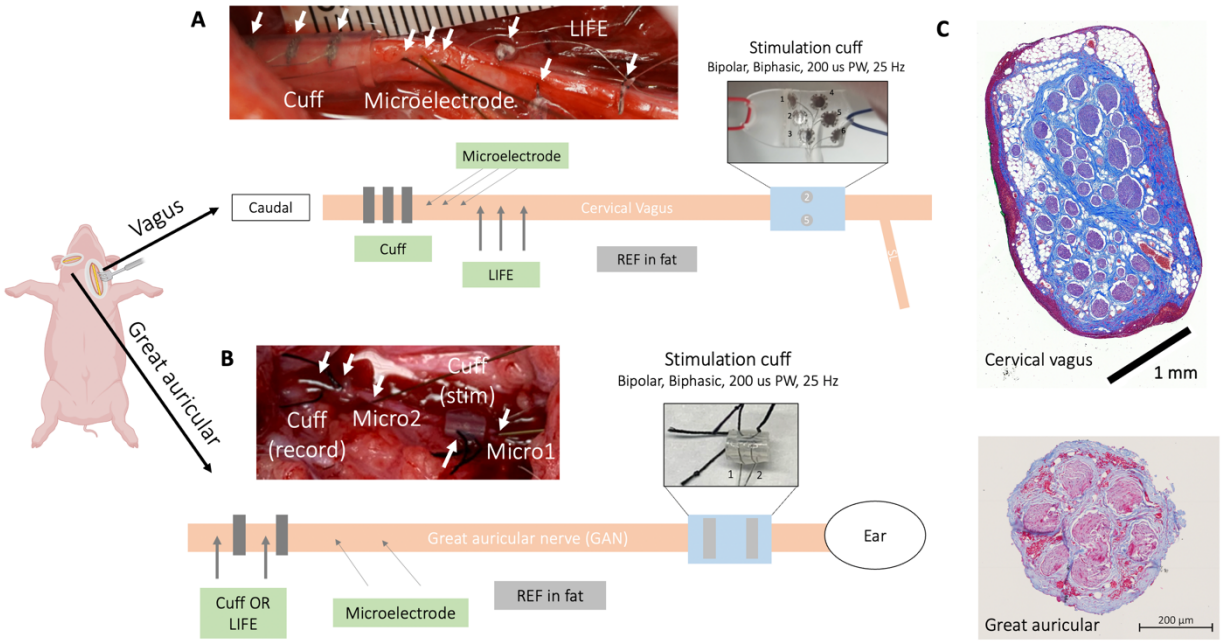

Figure 2: Experimental setup and surgical preparation.
(A) Cervical vagus nerve instrumented with bipolar stimulation cuff (contact 2 and 5) and, at least 4 cm caudal, with three replicates each of three different recording electrodes: three longitudinal intrafascicular electrodes (LIFEs), three microneurography microelectrodes, and a three-contact cuff. All recording electrodes were referenced to fat (off-nerve local tissue reference).
(B) Great auricular nerve (GAN) instrumented with bipolar stimulation cuff and two replicates each of two different recording electrodes: two microneurography microelectrodes, and either a two-contact cuff or two LIFE electrodes (alternated by subject). All recording electrodes were referenced to fat (off-nerve local tissue reference).
(C) Histology of cervical vagus nerve and great auricular nerve (GAN) under the stimulation cuff showing the vagus nerve is larger and has more fascicles. GAN histology from additional subjects is shown in Supplementary Material.

We created a surgical pocket that was larger than necessary as our approach was to find the pathway in which the sensory GAN could be identified and the association it played with the auricular motor component of the facial nerve (facial auricular nerves). Our preparation allowed us to follow the facial auricular nerves dorsal looking for the GAN traveling in association as well as following the lateral auricular vein ventrally to where the nerves and vein course together (surgical pocket photograph in Supplementary Material). The skin and subcutaneous fat were incised from the medial posterior margin of the ramus. A small notch was palpated at this point and indicated the approximate level of the stylomastoid foramen. Here the facial nerve exited and divided into its various branches (Getty, 1975) (more on facial nerve anatomy in Supplementary Material). The incision continued dorsal following a line posterior to the temporomandibular articulation and up to the medial base of the ear just inferior to the medial crus of the helix. This allowed us to follow the lateral vein through the base of the ear as a landmark for finding the sensory input for the exterior skin of the auricle. This incision exposed the superficial musculoaponeurotic system (SMAS), a superficial

fibromuscular layer that integrated with the superficial temporal fascia dorsally and platysma ventrally. The SMAS layer was divided along the posterior margin of the ramus and posterior margin of the temporomandibular articulation/zygomatic process to expose the subfascial level adipose tissue. This underlying adipose tissue along the posterior margin of the temporomandibular articulation was the location where we were able to isolate the GAN (more on GAN anatomy in Supplementary Material) and branches of the facial nerve (Getty, 1975; Lefkowitz et al., 2013; Yang et al., 2015; Sharma et al., 2017). Running in conjunction with these nerves were the lateral/caudal auricular artery and vein, matching the description of Duisit et al. (2017).

To determine which of the exposed branches were motor or sensory in origin we electrically stimulated each of the nerve branches to look for a motor response (200 μs pulse width biphasic pulses, 0.02-1 mA, 1 Hz). This is similar to the procedure used to localize a microneurography electrode into the desired fascicle (Macefield, 2021). When the sensory branch of the posterior auricular nerve was identified by no motor response it was instrumented with a stimulation cuff (Fig. 2B) and recording electrodes (two microneurography microelectrodes and a two-contact cuff or two LIFE electrodes) and verified by recording sensory evoked responses during stroking of the skin at the base of the auricle. Reference electrodes were placed similarly as described above in the vagus preparation and the same electrophysiology recording setup was used.

Sensory evoked neural activity was recorded by lightly stroking the region of the ear innervated by the GAN ('on-target') with a brush. A 90 second recording was made with the first 30 seconds where no stroking was delivered, the next 30 seconds where stroking was delivered in the 'on-target' region and the last 30 seconds where stroking was delivered in an 'off-target' region of the ear (tip of ear) where the GAN is not expected to innervate. The 'off-target' stroking served as a control to ensure that the light stroking applied to the ear did not transfer to the recording electrodes as motion artifact. Transcutaneous electrical nerve stimulation (TENS) electrodes cut to 2 x 2 cm in size were applied to the same region of sensory innervation of the GAN as identified by the recording of sensory evoked potentials and at the base of the ear through which the main trunk of the GAN courses.

Non-invasively evoked CAPs were recorded during application of stimulation waveforms with parameters identical to those reported in the cervical vagus section. Invasively evoked CAPs were recorded during delivery of 750 biphasic stimulation pulses with a 200 μs pulse width at 25 Hz with stimulation amplitudes between 0 and 3-10 mA (determined based on each subject's motor threshold) presented in a randomized order. Time locked recordings were made through the recording electrodes.

Electrophysiology data analysis

A custom-built and publicly available Python package, PyeCAP (https://github.com/ludwig-lab/pyeCAP), was used for offline analysis of electrophysiology and physiology data.

Filtering

Electrophysiology data for ECAP analysis was filtered with a high pass 1st order Butterworth filter with a corner frequency at 100 Hz and a low pass Gaussian filter with a corner frequency at 3 kHz. The low pass gaussian filter negates the possibility of introducing filter 'ringing' artifact, which may be introduced by a Butterworth filter that has an 'overshoot' to an impulse response (Bovik and Acton, 2005). The stimulation artifact approximates an impulse, and an overshoot following a stimulation artifact – caused by inappropriate filter selection – could be mistaken for an ECAP. An additional 60 Hz band stop finite impulse response (FIR) filter constructed with a Hamming window was used on the electrophysiology data for analysis of sensory evoked and spontaneously occurring neural activity. All filtering was performed on the time series data in both the forward and backward direction to eliminate group delays caused by filtering (Scipy, 2022).

Non-functional recording electrodes

As per the pre-registration (https://osf.io/y9k6j), non-functional recording electrodes were identified by a high noise floor, high 60 Hz noise, or a flat dose-response behavior in the ECAP signal in comparison to other contacts of the same electrode type. Electrodes deemed non-functional by these criteria were noted (see Supplementary Material) and removed from analysis.

Detecting Authentic ECAPs

ECAPs were plotted by averaging (point by point median) the stimulation evoked response across all available consecutive pulses in a particular stimulation train. Averaging of multiple stimulation evoked responses (n) reduces uncorrelated noise by a factor of $\sqrt{n}$ (Metcalfe et al., 2018). The averaged ECAP traces were split into time windows by neural fiber type according to the distances between recording and stimulation electrode and published conduction velocities (Erlanger and Gasser, 1937; Manzano et al., 2008).

ECAP authenticity was confirmed by several methods. Firstly, signal propagation delay across recording electrodes (Gaunt et al., 2009) was verified to be in the expected nerve fiber conduction velocity range (Erlanger and Gasser, 1937; Manzano et al., 2008). An artifact (e.g., EMG, motion) could occur at a similar time point as an ECAP but would not show up with a signal propagation delay across spatially separated recording electrodes. Secondly, a muscle paralytic, vecuronium, was used to abate EMG artifact in the ECAP recordings. Thirdly,

transection of the nerve between the stimulation and recording electrode and subsequent recordings were used to confirm the disappearance of the ECAP signal, which is no longer able to propagate along the transected neural pathway from stimulation to recording electrode (Nicolai et al., 2020).

Quantifying ECAP magnitude

Aβ- and B-fiber ECAPs were quantified to investigate their magnitude as recorded by the microneurography, cuff, and LIFE electrodes. Aβ-fibers were selected as a measure of faster conducting myelinated fibers and B-fibers were selected as a measure of slower conducting myelinated fibers.

Time windows corresponding to Aβ- and B-fiber ECAPs were calculated for each electrode based on distance from that recording electrode to the stimulation electrode and published values of conduction velocity: 30-70 m/s for Aβ-fibers and 3-15 m/s for B-fibers (Erlanger and Gasser, 1937; Manzano et al., 2008). A tolerance of up to 20% was allowed on the conduction velocity if the ECAP was truncated by the initially calculated time window. Then, the fiber-type time windows were further narrowed, without removing the ECAP signal of interest, to be of equal duration across recording electrodes. This was critical to avoid bias that would arise with increasing distance of the recording electrode from the stimulation electrode and hence a longer computed time window over which the ECAP magnitude calculation is performed – possibly leading to a skewed ECAP magnitude measurement. Root mean square (RMS) was calculated on the narrowed fixed-duration window and used as a measure of ECAP magnitude. RMS was selected over alternative methods (e.g., integral or area under the curve) as it indicates the equivalent steady state energy value of an oscillating signal and represents the noise floor of the recording electrode (Rawlins, 2000), a useful measure, even when no ECAP signal is present at subthreshold stimulation currents. Furthermore, the measure of peak-to-peak voltage is more susceptible to noise and amplitude is susceptible both to noise and baseline offsets (Mitra et al., 2018).

Detrending neural signal from stimulation artifact

Neural signal was detrended from stimulation artifact using an exponential based 'fit and subtract' approach (Harding, 1991; Chakravarthy et al., 2022; Drebitz et al., 2020). A simple method was used as only ECAPs from Subject 6 microneurography microelectrode recordings during the vagus dose-response experiment were contaminated by stimulation artifacts. A single exponential decay of the form:

$$y = Ae^{-b(x+c)}$$

with free parameters a, b, and c were used to fit ECAP data points between 2.2-2.4 ms and 5.8-6.0 ms using the method of least squares. This time range excluded ECAPs from fiber types of

interest. A representative fit is shown in Supplementary Material. The fit was subtracted from the raw ECAP trace to produce a detrended ECAP trace, which was used for further quantification of ECAP magnitude as described earlier.

Spike detection

Spike detection was done using a voltage thresholding method. The threshold voltage was set per electrode at six times the standard deviation (SD) from time=1-6 seconds of the time series trace recorded by that electrode added to the mean calculated from the same time window (time=1-6 seconds) to account for baseline offsets.

Cohort-based statistics

For ECAP magnitudes and spike counts, the mean value was taken for the replicate contacts of each type of electrode per subject. These mean ECAP magnitudes and spike counts measured on each electrode were normalized to the mean value measured on the cuff contacts and microneurography microelectrode contacts respectively, per subject, to facilitate comparison across subjects. Log10 was applied to the normalized values to redistribute to normality (Chen, 1994). The Shapiro-Wilk test was used to verify the normality assumption of the student t-tests. One-sided t-tests were used to test the hypothesis that 1) the Aβ-fiber ECAP magnitude recorded on the cuff was greater than that recorded on the microneurography microelectrode and 2) greater than that recorded on the LIFE electrode. Similarly, the hypothesis was tested that 3) the spike count from the microneurography microelectrode recording was greater than that from the LIFE electrode recording and 4) greater than that from the cuff electrode recording. Following the pre-registration, $\alpha = 0.05$ was used in a sequential analysis and propagated down the four primary outcomes listed above and then the secondary outcomes till a null result was hit. Confidence intervals (CI) were calculated using the 95% bounds of the t-distribution. Mean is denoted as μ and standard error is denoted as (SE).

Dose-response curves

Dose-response plots for the cervical vagus nerve were generated by plotting ECAP magnitude against stimulation current. The Aβ-fiber dose-response curve for each recording electrode was normalized to the ECAP magnitude at 5 mA of stimulation current for that recording electrode as it was the highest common stimulation current used across all subjects. Logistic growth functions (sigmoidal shape) were used to fit the dose-response curves with the method of least squares (Castoro et al., 2011). After subtracting the initial offset from the fitted logistic growth functions, EC10 points were calculated for each of the three electrodes for all n=6 subjects. The EC10 point is the stimulation current at 10% of the saturation ECAP magnitude and is a measure of the stimulation level at which the ECAP is first detectable. A repeated measures ANOVA

between the three recording electrode types was used to detect if the EC10 point, and hence sensitivity to ECAP detection, is different with recording electrode type.

Results

In this study, we characterized the performance of three commonly used electrodes (i.e., recording cuff, microneurography microelectrode, and intrafascicular electrode) to record neural activity from the peripheral nervous system. Both electrical stimulation evoked CAPs and sensory evoked neural activity induced by sensory stroking were investigated. For stimulation evoked CAPs, we characterized the recording electrodes on their capabilities to record invasive cuff stimulation evoked CAPs and non-invasive TENS evoked CAPs. These results provide the first side-by-side comparison in a human-scaled large animal model on the recording magnitude, sensitivity, and noise floors of the various recording electrodes in the peripheral nervous system. Further, we report on several referencing strategies and their appropriate use. Lastly, we highlight several artifacts in our recordings that initially appeared as neural signals but were later rejected by appropriate controls. We intend the results of this study to guide the development of neural recording techniques to be used in the deployment of neuromodulation therapies. Direct measures of on- and off-target neural recruitment around the stimulation electrode could help with the understanding of therapeutic mechanisms and guide adjustments to electrode design and placement to tune stimulation specificity. Neural activity recordings may also enable closed-loop titration and operation of neuromodulation therapies.

Data associated with this study were collected as part of the Stimulating Peripheral Activity to Relieve Conditions (SPARC) project and are available through the SPARC Data Portal (https://doi.org/10.26275/vm1h-k4kq) under a CC-BY-4.0 license.

Measuring ECAPs during invasive stimulation

Neuromodulation therapies can lack specificity of target engagement (Heusser et al., 2016; De Ferrari et al., 2017). In these therapies, the ability to directly measure neural activation around the stimulation site and understand fiber types activated could be critical to understand mechanism of action and enable electrode contact position adjustments to enable a more efficacious therapy (Verma et al., 2021a). Such measurements of local neural target engagement could be done either acutely in the doctor's office during placement and titration of the therapy or chronically implanted with the therapy device. For the former, a microneurography microelectrode – already in common clinical research use – could be percutaneously introduced to the nerves of interest (Ottaviani et al., 2020). For the chronic case, with an already invasive device, a recording cuff electrode could be implanted on the nerve of interest during the surgery to place the stimulation electrode.

Here, we compare these two clinically viable options (i.e., microneurography microelectrode and invasive recording cuff) to record ECAPs in the cervical vagus nerve of the domestic swine. Alongside, we compare a commonly used pre-clinical electrode, the LIFE (Yoshida and Stein, 1999; Nicolai et al., 2020). The electrodes were compared to characterize their ECAP recording magnitudes, sensitivities, and noise floors.

Magnitude of ECAP recorded

We characterized the magnitude of the ECAP recorded on each electrode. In general, a larger magnitude signal requires less demanding electronic design to record than a smaller magnitude signal. Representative traces are shown in Fig. 3A. ECAPs were recorded concurrently on all three types of recording electrodes (3 contacts each, for a total of 9 recording contacts per subject) at 1.5 mA of stimulation. The stimulation current was selected because it was close to the saturation point of Aβ fibers and provided a stable point of comparison across subjects (n=6).

Fig. 3B shows the magnitude of ECAP recorded by each of the recording electrodes during cervical vagus nerve stimulation (VNS). The magnitude of the ECAP recorded by the cuff was significantly larger than that of the microneurography microelectrode (normalized to cuff $\mu = 0.208\ SE = 0.088\ \mu V_{rms}/\mu V_{rms}$) ($p = 0.002, \alpha = 0.05, CI = [0.052, 0.343]$). Similarly, the magnitude of the ECAP recorded by the cuff was significantly larger than that of the intrafascicular electrode (normalized to cuff $\mu = 0.335\ SE = 0.077\ \mu V_{rms}/\mu V_{rms}$) ($p = 0.003, \alpha = 0.05, CI = [0.147, 0.541]$).

Sensitivity of recording electrodes

The sensitivity of a recording electrode is critical when it is used to detect the threshold of neural activation, which is a plausible use case in closed-loop control designed to avoid an off-target effect. The sensitivity of the three recording electrodes was quantified by constructing dose-response curves using 16-18 stimulation current doses between 0-10 mA, fitting to a logistic growth function, and calculating stimulation current at 10% of the maximal ECAP magnitude (EC10) as a measure of when an ECAP is first detectable. The mean was taken for the three replicate contacts of each type of electrode per animal before fitting.

Fig. 3D summarizes the EC10 point of each recording electrode across all subjects (n=6). The microneurography microelectrode had the lowest mean EC10 stimulation current, suggesting it was the most sensitive recording electrode. However, variability was large and the individual data plots showed that the microneurography microelectrodes were not consistently the most sensitive electrode in every subject. A repeated measures ANOVA test concluded non-

significant differences in EC10 currents across recording electrode type ($p = 0.26, \alpha = 0.05$). Repeating the analysis using the EC50 point confirmed a similar trend with non-significant difference results (data not shown). Due to this non-significant result, Type II error was entirely lost at this secondary outcome and further conclusions in the sequential analysis (see pre-registration) are exploratory, indicated by ($\alpha = 0$) where applicable. Note that the study was powered for the primary outcomes (as reported in the pre-registration) and not this secondary outcome on sensitivity.

Since sensitivity was evaluated by fitting to multiple points in the dose-response curve, it was a measure of the electrodes 'denoised' performance and not reflective of the electrodes' ability to detect the threshold of neural activation from a single level of stimulation current, which depends more critically on the signal-to-noise ratio (SNR).

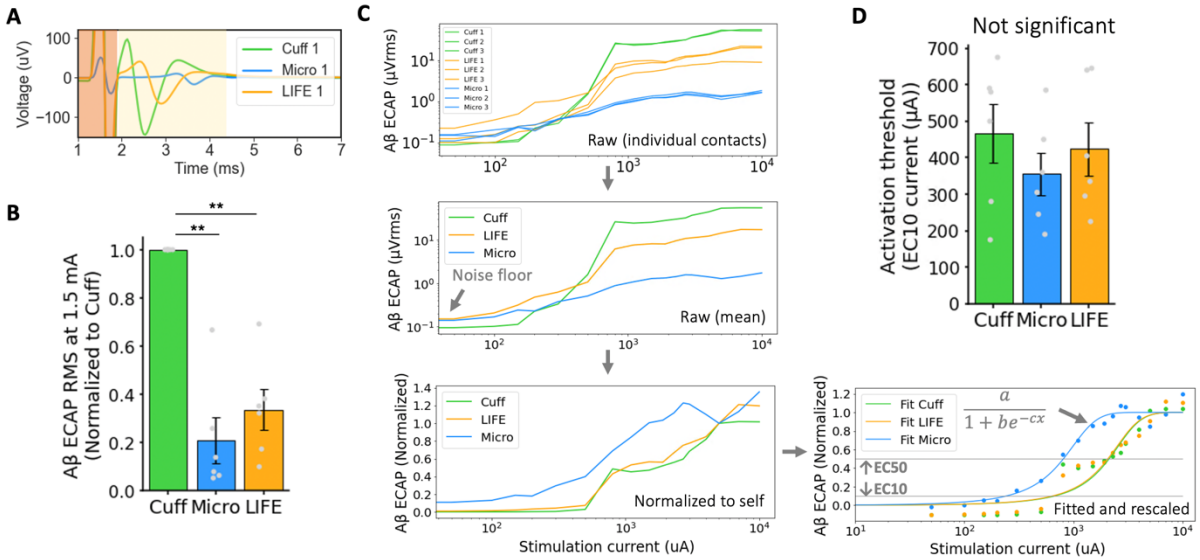

Figure 3: Electrode characterization for recording ECAPs from larger myelinated fibers.
(A) Representative ECAP traces from concurrent cuff, microneurography microelectrode, and intrafascicular recordings at 1.5 mA of stimulation on the cervical vagus nerve. Contact one of three was selected for each electrode type. Stimulation artifact shaded in orange and Aβ-fiber ECAP shaded in yellow.
(B) Bar plot summarizing magnitude of Aβ-fiber ECAP recorded with three different electrodes on cervical vagus showing significantly larger recording on cuff compared to both the microneurography microelectrode and intrafascicular electrode.
(C) (top left) Dose-response curves of Aβ-fiber ECAPs for three replicates each of the three recording electrode types characterized. From top left, in an anti-clockwise direction, shows the process of fitting dose-response curves with logistic growth function.
(D) Bar plot summarizing sensitivity of three different recording electrodes using their EC10 points representing stimulation current for 10% of saturation level neural activation – extracted from dose-response curve logistic growth function fits in **(C)**.

Noise floor of recording electrodes

The recorded ECAP magnitude and sensitivity of the recording electrode, along with the noise floor of the electrode, determine the electrode's practical performance in detecting the threshold of neural activation. The noise floor of each electrode was characterized by calculating the RMS signal across 5 seconds of time series (un-averaged) electrophysiology data both before (Fig. 4A) and after (Fig. 4B) filtering (low-pass and high-pass filters as reported in Methods section). The averaging done to construct ECAP traces reduces uncorrelated noise by a factor of $\sqrt{n}$, where n is the number of traces averaged (Metcalfe et al., 2018). The noise floor of ECAP traces (Fig. 4C) was characterized by reporting the RMS signal in the Aβ window range at 0 mA of stimulation (no stimulation delivered).

Fig. 4 shows the noise floor of all three recording electrodes before and after filtering in time series and after filtering in averaged (n=750) ECAP traces. As discussed earlier, the noise floor is higher in the time series and lower in the averaged ECAP traces (2.53 μV_{rms} vs. 0.11 μV_{rms} taking the recording cuff as an example) as expected. In the time series electrophysiology data, the noise is higher before filtering than after (15.85 μV_{rms} vs. 2.53 μV_{rms} taking the recording cuff as an example), largely due to the contribution of low frequency noise (Supplementary Material). The microneurography microelectrode has the highest noise floor across all three electrodes (0.26 μV_{rms} for the microneurography microelectrode vs. 0.11 μV_{rms} for the cuff and LIFE, taking the filtered ECAP noise floor as an example). In subject 5 and 6, an active head stage was used on the microneurography microelectrode, which pre-amplified the signal at the electrode, theoretically reducing SNR loss due to the noise picked up on the wire from the electrode to the main amplifier. However, in doing so, additional electronic noise was introduced by the pre-amplifier and is observed in the two higher noise data points in Fig. 4B (mean of 3.51 μV_{rms} for subjects 1-4 vs. 8.77 μV_{rms} for subjects 5-6, taking the filtered time series as an example). In the discussion section, we further discuss the sources of noise (i.e., environmental, biological, electrochemical, and electronics) for each recording electrode.

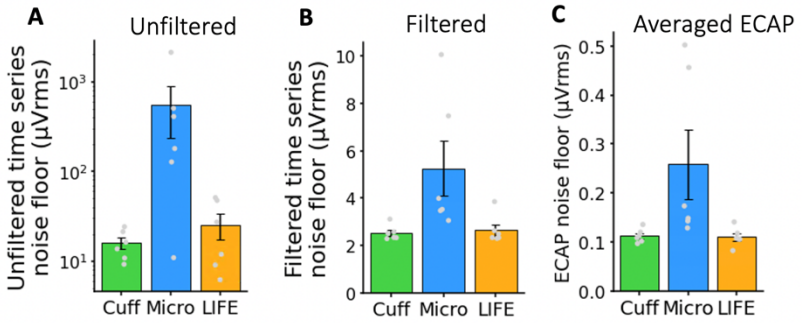

Figure 4: Nose floor of recording electrodes.
Noise in electrophysiology recordings showing largest noise levels on the microneurography microelectrode. Note the differing y-axis scales in the three sub panels as the noise level after filtering and averaging is reduced by orders of magnitude.
(A) Unfiltered time series electrophysiology.
(B) Filtered time series electrophysiology.
(C) Filtered averaged (median) ECAPs.

B-fiber recordings on recording electrodes

Several neuromodulation therapies posit small diameter fibers are responsible for their therapeutic effect. For example, B-fibers in the heart failure applications of VNS (Sabbah et al., 2011) are smaller diameter myelinated fibers. Due to the smaller fiber size and signal magnitude, they are more challenging to record from (Yoo et al., 2013; Nicolai et al., 2020). We compared the three recording electrodes (cuff, microneurography microelectrode, and intrafascicular electrode) in their ability to record B-fibers from the cervical vagus nerve. Vecuronium was administered at a sufficient dose in subjects 4-6 to blunt EMG artifact from contaminating the neural recordings. Insufficient vecuronium was available in subjects 1-3 due to a protocol modification. B-fibers were confirmed by signal propagation delay across the replicate contacts of each electrode type (Fig. 5A, inset). It was not possible to conclude that we were quantifying only B-fibers because of the overlap of B-fibers and Aδ-fibers in the conduction velocity ranges (Erlanger and Gasser, 1937; Manzano et al., 2008). However, the purpose of this analysis was only to contrast slower conducting myelinated fibers (B/Aδ) with the previous faster conducting myelinated fibers (Aβ) to capture any differences in ECAP magnitude across the recording electrodes by fiber type and hence widen applicability of the results.

B-fiber ECAPs were most consistently recorded on the cuff, only evident in certain subjects with the intrafascicular electrode, and notably less evident with the microneurography microelectrode. Fig. 5A shows B-fiber ECAP traces confirmed by signal propagation delay across two cuff contacts. A similar plot as Fig. 5A, shown in Supplementary Material, suggests authentic B-fiber ECAPs recorded on the intrafascicular electrode but not the

microneurography microelectrode. Fig. 5B and 5C show dose-response curves for B-fiber ECAPs and stimulation-evoked bradycardia, respectively. B-fibers are putatively responsible for decreases in heart rate during VNS (Qing et al., 2018). The bradycardia dose-response curve best tracks the cuff B-fiber recordings up to ~2 mA. After that, afferent pathways may be recruited balancing the efferent B-fiber mediated effects (Ardell et al., 2017). The cuff B-fiber ECAP recordings correlate best with stimulation-evoked bradycardia in this subject (R_cuff = 0.70 and R_LIFE = 0.39). Data from remaining subjects are shown in Supplementary Material.

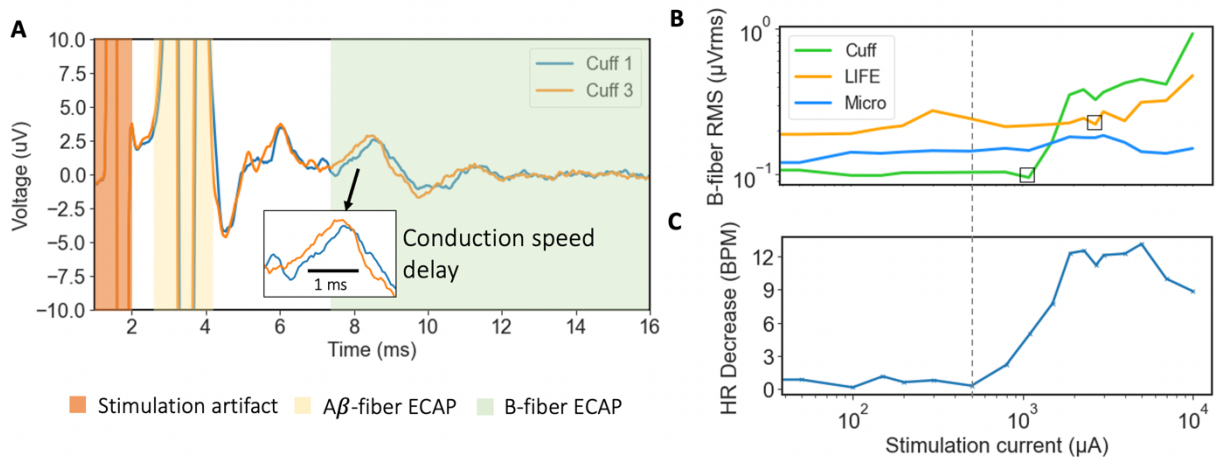

Figure 5: Electrode characterization for recording ECAPs from smaller myelinated fibers.
(A) Authenticity of B-fiber recordings was confirmed by signal propagation delay across recording electrodes in the range of 3-15 m/s (Erlanger and Gasser, 1937; Manzano et al., 2008). An artifact (e.g., EMG, motion) could occur in a similar time window but would not show up with a signal propagation delay across spatially separated recording electrodes. Stimulation artifact shaded in orange, Aβ-fiber ECAP shaded in yellow, and B-fiber ECAP shaded in green. Stimulation was delivered at 10 mA. A similar plot is shown for the intrafascicular and microneurography electrode in Supplementary Material.
(B) B-fiber dose-response curves for all three recording electrodes on a single subject showing the largest ECAP magnitude recorded with the cuff electrode. The cuff electrode also recorded ECAPs at the lowest stimulation current. The ECAP detection threshold for each electrode is boxed; a clear threshold was not recognized on the microneurography microelectrode. The dash line from **(C)** indicates the bradycardia onset threshold.
(C) Heart rate decrease (bradycardia) dose-response curve in the same subject as (b) showing bradycardia stimulation current threshold is slightly lower than the B-fiber recording thresholds in (b). Bradycardia dose-response curve best tracks the cuff B-fiber recordings up to ~2 mA. After that, afferent pathways may be recruited balancing the efferent B-fiber mediated effects (Ardell et al., 2017).

Reference electrode on nerve versus in surrounding non-neural tissue

Judicious choice of reference electrode (e.g., local tissue or on-nerve reference) can optimize neural signal fidelity and minimize artifact. Neural recordings can be referenced to a location on the active nerve itself or in surrounding non-excitable tissue. Conventionally, cuff electrodes have been referenced on the nerve (e.g., bipolar or tripolar) while in microneurography, the

reference is placed in surrounding non-neural tissue (Macefield, 2021). We conducted ECAP recordings with different referencing strategies and systematically compared 'on-nerve' references with 'local tissue' reference.

Fig. 6A shows that local tissue referenced recordings have a much larger stimulation artifact than on-nerve referenced recordings, but also a ~2.5x larger ECAP peak-to-peak magnitude. Stimulation artifacts in local tissue referenced recordings may be minimized by placing the reference electrode equidistant from the stimulation electrode as the active recording electrode. The smaller magnitude ECAP recorded with on-nerve reference can be explained by 'subtraction' of neural signal between the active and reference electrode due to the 2-3 cm wavelength of the Aβ-fibers that appears common to both electrodes (Andreasen and Struijk, 2002).

The ECAP can be visualized as a moving electric dipole with the negative depolarizing charge leading the positive repolarizing charge (Fig. 1B). The distance between the poles is the 'wavelength' of the ECAP and for myelinated fiber types is approximately the conduction velocity specific to the fiber type multiplied by ~1 ms (the duration of an action potential). For smaller fibers with slower conduction velocities and shorter wavelengths, this subtraction should not be evident when the wavelength is less than the distance between the recording and reference contacts on the nerve. As such, on-nerve reference might be beneficial when recording smaller fiber diameters, with shorter wavelengths, as ECAP magnitude is persevered while common mode artifact is reduced.

Tripolar versus bipolar on-nerve referencing strategies with recording cuff

An on-nerve reference close to the active recording electrode can efficiently reduce common-mode artifacts external to the electrodes, such as spillover electric field from muscle activity and stimulation artifact (Sabetian et al., 2017). On-nerve reference strategies lend themselves to cuff recording electrodes and are typically employed in a bipolar or tripolar configuration. Past works have shown several key differences between tripolar (contact 1 and 3 tied together to reference, contact 2 used for recording) and bipolar referenced cuff recordings (Sabetian et al., 2017). Namely, tripolar referencing reduces the representation of common mode artifacts (Sabetian et al., 2017), which is pertinent as these artifacts can appear at similar time points as neural fiber signals (Nicolai et al., 2020). However, bipolar cuffs, compared to tripolar cuffs, can detect neural signal propagation direction (afferent vs. efferent). Meanwhile, the magnitude of neural signal recorded by the bipolar vs. tripolar cuff depends on the geometry of the cuff. In particular, the electrode length (EL) and electrode edge length (EEL) of the insulation, as reported in a computational modeling study (Sabetian et al., 2017).

We collected both tripolar and bipolar referenced recordings using the same cuff. Fig. 6A shows representative bipolar and tripolar traces at 2.3 mA of stimulation. The stimulation artifact magnitude is smaller in the tripolar compared to the bipolar reference. The peak-to-peak ECAP magnitude is also smaller in the tripolar reference by a factor of ~2.2x compared to the bipolar reference. Data from other subjects are shown in Supplementary Material and support the conclusions reported here. Our experimental results support the computational results reported by Sabetian and colleagues (2017) with an EL of 9 mm and an EEL of 2 mm predicting a ~1.4x larger peak-to-peak neural recording on the bipolar reference compared to the tripolar reference. Note these results are dependent on the cuff geometries, which are further explored in the computational work by Sabetian and colleagues (2017).

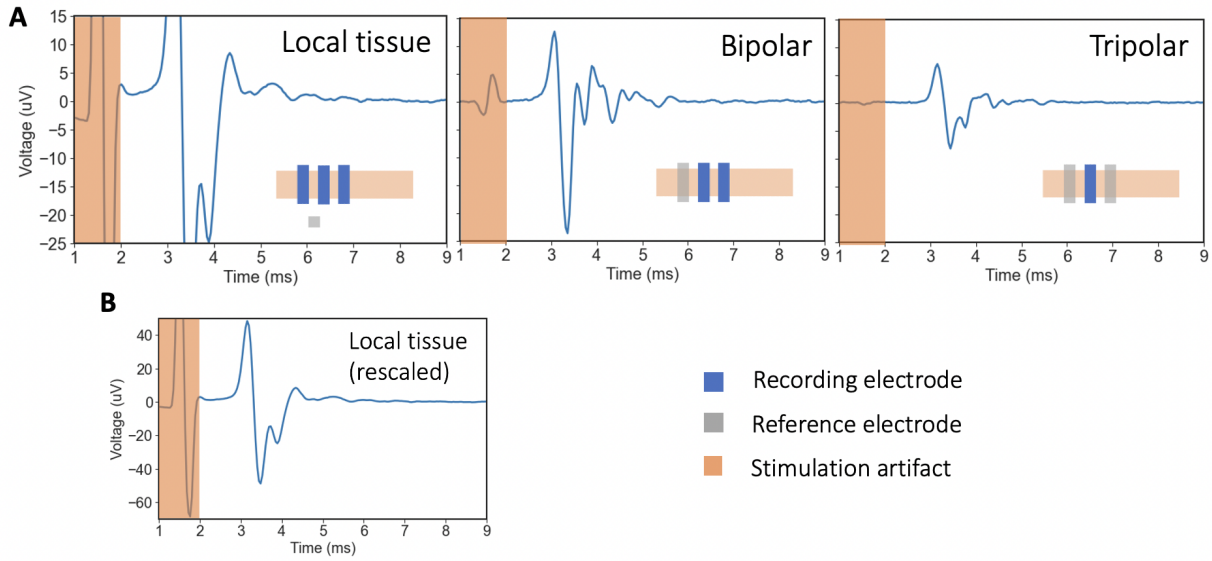

Figure 6: Referencing strategies.

(A) Representative data showing ECAP traces with three different referencing strategies at 2.3 mA of stimulation: (left) reference in 'local tissue', (center) bipolar 'on-nerve' reference, and (right) tripolar 'on-nerve' reference. Orange highlights overlap the stimulation artifact, an example of common mode noise, which is substantially reduced in the on-nerve referencing strategies. The Aβ-fiber ECAP (~3-4 ms) is also smaller in the 'on-nerve' reference strategies due to the longer wavelength of Aβ-fibers appearing common on both the recording and reference contact and being subtracted off. In the illustration of the recording setup in each plot, blue indicates recording electrodes and gray indicates reference electrodes.

(B) Rescaled plot of 'local tissue' reference from **(A)** to show full y-axis scale illustrating substantially larger Aβ-fiber ECAP recorded with local tissue reference.

Measuring sensory evoked neural activity

Changes in spontaneously occurring neural activity could be a sensitive and real-time marker for neuromodulation therapies (Gonzalez-Gonzalez et al., 2021; Chao et al., 2021). Measuring spontaneous activity may be especially important in cases when there is an afferent-efferent

pathway with one or more synaptic connections, introducing variable conduction latency and desynchronizing the timing of the neural signal, thereby preventing a clear ECAP from appearing in the later efferent pathway. Instead, changes in spontaneously occurring neural activity of the later efferent pathways can be a sensitive measure of therapy effect and can be used for therapy titration. Recording spontaneous activity may also be important for non-traditional waveforms such as burst, pink noise, high frequency block, or direct current (DC) block where the timing of initiation of an action potential may be variable or moot, and the intended effect is to change spontaneous activity in between stimulus trains. Consequently, we compared the three types of recording electrodes in their ability to measure sensory evoked neural activity, also an asynchronous neural signal, from the great auricular nerve (GAN), implicated as an on- or off-target nerve in various auricular stimulation-based therapies.

Fig. 7B shows representative data of the sensory evoked neural activity recordings made with a cuff electrode, microneurography microelectrode, and intrafascicular electrode during a 30 second quiescent period, 30 seconds of on-target stroking at a region of the auricle innervated by the GAN (Fig. 7A), and 30 seconds of off-target stroking at a region of the auricle not innervated by the GAN (Fig. 7A). The on- and off-target stroking was used to verify the authenticity of the sensory evoked neural recordings. The representative recording from the intrafascicular electrode showed spike-like activity throughout the 90 second recording period. The shape of the spike (Fig. 7C) and the synchronization of the timing with the ventilator indicated that the spike activity on the intrafascicular electrode was due to motion artifacts from the ventilator. Transection of the GAN was also attempted as a control to verify the authenticity of the neural recordings. However, due to the webbed nature of the nerve at the insertion point to the ear, we were unable to completely transect it in every subject to eliminate the sensory evoked neural activity.

Spikes on each electrode were detected using the thresholding method described in the Methods and the median was taken for the two replicate contacts of each type of electrode per subject. To pool results across subjects, the LIFE and cuff electrode spike count in each subject was normalized to the microneurography microelectrode spike count in that same subject.

Fig. 7D bar plot summarizes the spike count on each recording electrode (normalized to the microneurography microelectrode in that subject) during on-target sensory stroking of the region of the auricle innervated by the GAN. The microneurography microelectrode spike count was significantly larger than that of the cuff (cuff spike count normalized to microneurography microelectrode $\mu = 4.38 \times 10^{-3}$ $SE = 2.43 \times 10^{-3}$) ($p = 0.01, \alpha = 0.05, CI = [5.22 \times 10^{-5}, 6.34 \times 10^{-2}]$). Similarly, the microneurography microelectrode spike count was significantly larger than that of the intrafascicular electrode (intrafascicular spike count

normalized to microneurography microelectrode $\mu = 1.95 \times 10^{-2}$ $SE = 2.7 \times 10^{-3}$) ($p = 0.001, \alpha = 0.05, CI = [9.38 \times 10^{-3}, 3.76 \times 10^{-2}]$). Further recordings made on another nerve, the cervical vagus nerve, during spontaneously occurring activity did not produce consistent and sustained neural spikes on any of the recording electrodes tested – and is discussed further in the discussion section.

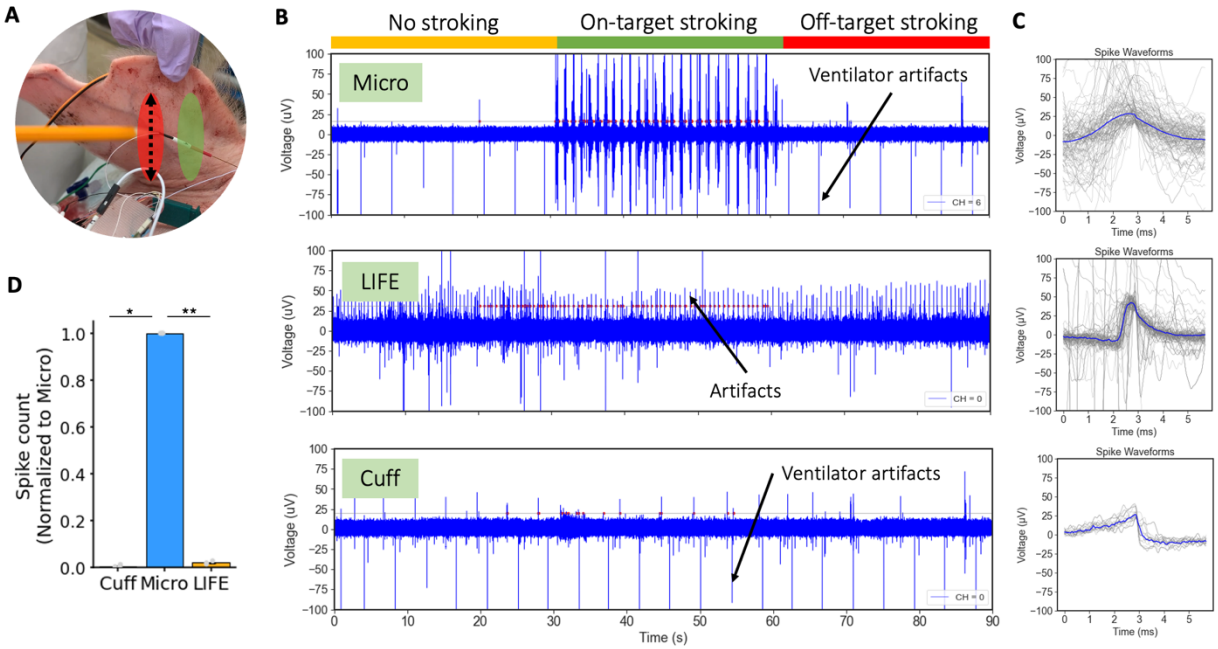

Figure 7: Electrode characterization for recording sensory evoked neural activity (sensory evoked).
(A) Stroking ear at off-target (red, not innervated by GAN) and on-target (green, innervated by GAN) areas corresponding to green and red color coding in **(B)**.
(B) Representative 90 seconds of electrophysiology recordings: first 30 seconds with no stroking, middle 30 seconds with on-target stroking, and last 30 seconds with off-target stroking to control for motion artifacts from stroking. Only the microneurography microelectrode shows a robust response specific to on-target stroking. LIFE and cuff traces were selected to illustrate artifacts that were present in recording, which appeared neural, but were not authenticated by multiple controls including administration of a muscle blocker to reduce tremoring (tremoring shown here in the LIFE recording).
(C) Spike shapes for each electrophysiology trace shown in **(B)** indicating multi-unit hash recordings on the microneurography microelectrode, tremoring artifact on the LIFE, and ventilator artifact on the cuff electrode.
(D) Bar plot summarizing spike count recorded by three electrodes (data from all subjects) showing the microneurography microelectrode records significantly more spikes than both the cuff and LIFE.

Artifacts in electrophysiology recordings

We applied several controls to differentiate artifacts from bona-fide neural signals. These included: administration of a muscle paralytic, nerve transections, verifying signal propagation delay across contacts, concurrent monitoring of heart rate and respiration to investigate synced 'neural' activity, inspection of waveform shapes, and controls for induced motion. Through this

appropriate use of controls, we classified several signals that initially appeared neural as non-neural artifacts. Specifically, in time series (non-averaged) recordings we identified artifacts from respiration, cardiac, and tremor related effects.

Firstly, respiration related artifacts are captured in Fig. 7B (Cuff) occurring at a rate of once every ~4s (15 times/minute) in sync with the respiration rate set on the ventilator. The artifact did not go away with nerve transections and had a unique spike shape (Fig. 7C, bottom panel versus sensory evoked activity in top panel). The ventilator-induced artifacts likely occurred due to motion of the animal with respiration. Secondly, tremoring related effects are observed in Fig. 7B (LIFE). Tremoring of the subject is described in the Methods. These motion related artifacts from tremoring disappeared with the administration of vecuronium, a muscle blocker, or the anesthetics Telazol or Ketamine, all of which stopped the tremors. Lastly, cardiac related artifacts were recorded (shown in Supplementary Material), which were removed with high pass filtering at 100 Hz. Cardiac artifacts can be directly from electrocardiogram (EKG) or from cardioballistic effects due to the beating motion of arteries adjacent to the nerve (Ulrich et al., 2016) that cause motion in the nerve and the recording electrode. The cardioballistic effect was visible to us in several instances and is synced with heart rate. Direct EKG may be a more likely source of the artifact if the recording and reference electrode pair are across the heart or generally separated by a larger distance. The susceptibility of all three recording electrodes to motion induced artifacts suggests that one needs to be careful in interpreting spontaneous neural activity recordings in response to physiological events that also create motion, such as respiration, cardiac activity, etc.

Discussion

We reported on a side-by-side comparison of neural recording electrodes for the peripheral nervous system in a human-scaled large animal model. We compared cuff electrodes, microneurography microelectrodes, and intrafascicular electrodes by collecting recordings of 1) cuff evoked CAPs, 2) TENS evoked CAPs, 3) sensory evoked neural activity, and 4) spontaneously occurring activity. The cuff recordings measured Aβ- and B-fiber ECAPs with the highest SNR. However, when a range of stimulation currents were delivered to create a dose-response curve, the microneurography microelectrode detected Aβ-fiber ECAPs at the lowest stimulation current. The microneurography microelectrode was also the only electrode to record clear sensory evoked neural activity. TENS evoked CAPs were not recorded by any of the recording electrodes, which is discussed in detail later in this section. We compared 'local tissue' reference with 'on-nerve' reference options and observed larger ECAP magnitudes with the 'local tissue' reference compared with 'on-nerve' references, albeit with larger common mode artifacts.

In the discussion, we first summarize the strength and weaknesses of different recording electrodes and discuss suitable electrode type and referencing strategies per application. Secondly, we outline potential mechanisms of neural recording to explain the results. We then discuss challenges in recording spontaneously occurring activity and TENS evoked CAPs in relation to past work. Next, we discuss sources of noise in electrophysiology recordings. Lastly, we discuss correlation of ECAP magnitudes recorded on the three electrodes with evoked cardiac responses.

Electrode choice by application

In the context of neuromodulation therapies, ECAPs can be used as a real-time and precise measure of local target engagement around the stimulation electrode (Verma et al., 2021a). Several neuromodulation therapies are critically limited by off-target nerve engagement (Heusser et al., 2016; De Ferrari et al., 2017), which may be addressed by electrode design and stimulation parameters. Electrode design and stimulation waveforms are often ported directly from animal models and not adjusted for human use due to lack of real-time measures to guide development. We believe ECAPs represent a readily available method to develop and deploy neuromodulation therapies in patients to improve on-target engagement and consequently therapeutic efficacy. Table 1 summarizes the performance and utility of the different recording electrodes based on the outcomes of the experiments performed in this study.

Table 1: Recording electrode choice by application

	Large diameter fibers ECAP	Small diameter fibers ECAP	Asynchronous neural activity	Chronic recording interface	Minimally invasive introduction	Noise floor
Microneurography microelectrode						
Recording cuff						
LIFE						

*Green indicates good performance while orange indicates poor performance

Use of microneurography microelectrodes to develop and deploy minimally invasive neuromodulation therapies

Our data showed that recordings made using microneurography microelectrodes consistently measured Aβ-fiber ECAPs. In fact, once a full ECAP dose-response curve was constructed and fitted to overcome the SNR limitations of the microneurography microelectrodes, they showed the highest sensitivity in detecting an ECAP amongst the three recording electrodes tested. We also showed that recordings made using microneurography microelectrodes consistently

measured sensory evoked neural activity. Changes in spontaneously occurring activity could serve as a sensitive and real-time biomarker of neuromodulation therapy induced physiological effects (Gonzalez-Gonzalez et al., 2021; Chao et al., 2021).

The microneurography microelectrode tested is already used in humans to record muscle sympathetic nerve activity (MSNA) from the common peroneal nerve (Macefield, 2021) and median nerve (Macefield, 2021) and, most recently, neural activity from the cervical vagus nerve (Ottaviani et al., 2020). Similar to this existing human use, a microneurography microelectrode may be inserted percutaneously during clinical trials and/or at the deployment of neuromodulation therapies to map sensory innervation (Meier et al., 2018) to determine non-invasive stimulation electrode placement. The temporarily inserted microelectrode can also measure stimulation evoked on- and off-target neural activation and that data can be used in real-time to adjust stimulation electrode position, design, and stimulation parameters (Verma et al., 2021a). To aid in the translation of the microneurography technique to routine clinical use, the technique needs to be easy to perform and should be deployed within minutes. Currently, the technique requires a skilled microneurography practitioner, and even then, can be time consuming to target specific fascicles in a nerve. When working with clinical patients, procedure time and ease of performance of the technique are critical for adoption. Automation, such as insertion based on force or electrical impedance (Kodandaramaiah et al., 2012; Park et al., 2018), can be used to guide the microneurography microelectrode into the nerve and specific fascicle, where necessary. The epineurium and perineurium have vastly different mechanical properties and may be ideal to differentiate between fascicles (Koppaka et al., 2022).

Use of cuff electrodes to provide high-fidelity chronic recordings

Our data showed that the cuff electrode recorded ECAPs with the highest SNR. The cuff was also the only electrode to consistently record smaller diameter myelinated fiber (e.g., B-fiber) ECAPs. In applications where a chronic recording interface is necessary and smaller fiber types are of interest, an implanted recording cuff would be a suitable option.

In closed-loop strategies that rely on detecting first activation of a particular fiber type, and time for averaging is limited, the high SNR of the cuff ECAP recordings will be advantageous. For example, in a waveform block strategy to activate smaller diameter fibers without activating larger diameter fibers, continuous monitoring of large diameter fiber activity will be required with a sensitive and immediate measure of first activation necessary so that the stimulation parameters can be quickly adjusted to subsequently block the activated large diameter fibers. This requires a high SNR recording from a single measurement, without averaging, which is provided by the recording cuff.

Referencing strategy

The results show that referencing strategy (i.e., on-nerve bipolar vs. on-nerve tripolar vs. local non-neural tissue) have a profound effect on recorded neural signal and artifact magnitude and morphology (Fig. 6). The microneurography technique lends itself to the local tissue reference (Macefield, 2021), resulting in larger amplitude neural signals recorded, which compensates for the lower ECAP magnitudes observed with the microneurography microelectrode. To minimize common mode noise, the microneurography microelectrode should be inserted approximately equidistant from the stimulation site and in fat. The reference electrode tip should also be of similar material and design to the recording electrode to match the representation of common mode artifact. The cuff electrode lends itself to on-nerve reference strategies, which reduces the magnitude of the neural signals recorded (Fig. 6A), due to 'subtraction' of the neural signal when it appears common on both the recording and on-nerve reference electrode, particularly of the larger fiber types (longer wavelength). See results section for a discussion on how the 'subtraction' effect is less prominent for smaller fiber types (with slower conduction velocities and shorter wavelengths) and larger contact spacing between the cuff recording and reference contact. We observed that the cuff records the largest neural signal magnitude, thereby balancing out the aforementioned 'subtraction' effect. The on-nerve reference strategies (bipolar and tripolar) were robust at rejecting common mode noise, which is critical in an out-of-clinic ambulatory setting. Therefore, we conclude that local tissue reference, which lends itself naturally to the microneurography recordings, and on-nerve reference, which lends itself naturally to the cuff recordings, are appropriate for use as such.

Mechanisms of neural recording

Surprising, although recordings made with the microneurography microelectrode showed the most distinct sensory evoked neural activity, they measured Aβ-fiber ECAPs with the smallest magnitude. In contrast, the recordings made with the cuff did not show distinctive measurements of sensory evoked neural activity but measured ECAPs with the largest magnitude. The sensitivity of the penetrating microneurography microelectrode may be explained by its proximity to the firing neural source. The larger ECAP magnitude on the recording cuff may be explained by the cuff more linearly summing the electric potentials from all neurons firing within it (Humphrey and Schmidt, 1990) while the microneurography microelectrode summing up potentials with a greater weight from neurons firing adjacent to the recording tip and a substantially reduced weight from neurons at a distance from the recording tip (Buzsáki, 2004; Khodagholy et al., 2015). In this manner, the microneurography microelectrode records a large signal from an adjacent neural source and a small signal from a further neural source, while the cuff records and sums moderate signals from throughout the nerve it is applied on.

Recording spontaneous activity

None of the electrode recordings showed clear and repeatable spontaneously occurring neural activity in the cervical vagus nerve (data not shown). This contrasted with the great auricular nerve (GAN) where sensory evoked activity was recorded clearly by the microneurography microelectrode. This also contrasted with past microneurography work, which showed spontaneous activity recordings from the cervical vagus of humans (Ottaviani et al., 2020). Several differences could have contributed to this. Firstly, the GAN has <10 fascicles compared to the cervical vagus, which has >20 (Fig. 2C), which could have led to a higher chance of introducing the microneurography microelectrode into the appropriate fascicle in the GAN when targeted generally towards the center of the nerve. Secondly, compared to the clinical recordings, which were done percutaneously, we had an open surgical preparation. This may have led to additional trauma during microneurography microelectrode insertion with less mechanical stability provided by surrounding tissue. Further, the largest spontaneous signals from the cervical vagus are expected to come from Aβ muscle afferents under muscle tone. The manipulation of these muscles and the application of the muscle relaxant, vecuronium, in our experiments may have substantially reduced neural signaling from these muscles compared to clinical recordings in awake subjects. Similarly, the sensory evoked neural activity on the GAN is expected from Aβ fibers, which are a large fiber type and produce larger extracellular signals than the smaller B and C fibers, which may be the only source of spontaneous activity remaining on the cervical vagus nerve under the mentioned surgical and anesthetic conditions.

It is surprising then that experiments in rodents have shown recordings of spontaneous activity from the cervical vagus with simple hook electrodes (similar to cuff but without insulation) (Silverman et al., 2018; Stumpp et al., 2020). The difference in nerve size and perineurium thickness between rodents and pigs or humans may explain these results (Koh et al., 2022). As illustrated in Fig. 1C, the neurons in a rodent are much closer to the recording cuff than in a pig or human. The shorter distance in rodents results in a stronger extracellular signal at the point of the recording cuff and larger amplitude neural activity recordings (Koh et al., 2022).

While clear sensory evoked neural activity was not evident on the macroelectrode (cuff and intrafascicular electrode) recordings on the GAN, it is possible that the neural signals were masked by the low SNR of the recordings. Studies have shown that further signal processing, for example, velocity selective addition of neural signals from multiple channels, can be used to improve the SNR and detect spontaneous neural activity in macroelectrode recordings of human-scaled peripheral nerves (Metcalfe et al., 2018). Such strategies may be considered if the conduction velocity of the fiber of interest is known and computational resources to implement the algorithm are not limited by the intended clinical application. The lack of spontaneous activity recordings using macroelectrodes versus microelectrodes is also seen in

the central nervous system, for example in this report in clinical patients undergoing surgery for a brain implant (Winestone et al., 2012).

Measuring ECAPs during non-invasive stimulation

Numerous non-invasive stimulation devices have hit the market in recent years. Several, claiming to stimulate nerves deep below the surface of the skin without activating superficial off-target nerves (Nonis et al., 2017; Verma et al., 2021b). Microneurography based studies (Ottaviani et al., 2020) to record non-invasive ECAPs from the intended on-target nerve and expected off-target nerves during delivery of the non-invasive stimulation could clarify the actual nerves responsible for effect and side effect in an already efficacious therapy. Then, in future deployment of the therapy, the same microneurography techniques can be used to customize electrode position to account for inter-subject variation in anatomy to ensure that the same on-target nerve is recruited in each patient – possibly increasing responder rates. Direct and real-time measures of local neural target engagement are critical as surrogate or indirect measures can be confounded by muscle activity (Feucht and Ward, 2021), poor time resolution, etc. (Verma et al., 2021a).

We used TENS electrodes (2 x 2 cm) to stimulate 1) the region of the ear innervated by the GAN and 2) the base of the ear through which the trunk of the GAN courses. Using up to 10 mA of stimulation current, we did not observe ECAPs on any of the three recording electrodes tested (data not shown). While this current density was comparable to the lower end of current densities used in aVNS clinical trials (Verma et al., 2021a), and should have been sufficient for perception, it may have been insufficient to create enough synchronous recruitment of neurons to record clear ECAPs. The larger surface area of the TENS electrodes lends to synchronous activation of fibers but at spatially distinct locations across the span of the electrode. As the neural signals propagate, they remain asynchronous and do not form a clear large magnitude ECAP. Janko and Trontelj (1980) reported on microneurography recordings from the median, radial, and ulnar nerve during non-invasive stimulation of the finger. They used a smaller surface area electrode, which would have lent to more synchronized recruitment of neurons and a clearer ECAP. These findings may have implications towards electrode design for non-invasive bioelectronic medicine therapies – especially if the mechanism of action is reliant on synchronous recruitment of neurons.

Sources of noise in electrophysiology recordings

Fig. 4 summarizes the noise floor of each recording electrode before and after filtering and with averaging for ECAP presentation. There are several key sources of noise in neural recordings. They are listed here in order from the external environment, the *in vivo* environment, the electrode, and finally the electronics:

- External noise capacitively and/or inductively coupled, conducted, or radiated in the case of higher frequency electromagnetic field, into the recording, including mains 50/60 Hz noise (Yasar, 2021).
- Biological noise consisting of background neural and other electrical activity in the body (Yang et al., 2009).
- Noise due to motion of the electrode relative to tissue (Simakov and Webster, 2010).
- Thermal noise, generated by thermal motion of charge carriers, and is dependent on electrode impedance (Yang et al., 2009).
- Electrochemical noise reflecting corrosion on the metal electrode and interaction of charged ions with the solution (Obot et al., 2019).
- Electronic noise including flicker noise, thermal noise, digitization noise, etc. (Molecular Devices, 2006).

We found electronic noise to dominate in our results of 0.1 – 3 kHz filtered time series relevant to peripheral ECAP and spiking activity. We measured the electronic noise of the TDT SIM head stage to be 1.95 μV_{rms}. The measurement was made by shorting the input to reference while the setup was in a Faraday's cage (to reduce pick up of external noise). The recorded time series trace was then filtered, and RMS noise was calculated as it was for *in vivo* recordings. Our measurement of the input referred noise floor was similar to that reported in the TDT SIM head stage datasheet (TDT, 2022) adjusted for the appropriate bandwidth. *In vivo* measurement of noise from the recording cuff filtered time series trace is 2.53 μV_{rms} on average, which suggests that ~77% of RMS noise is from recording electronics front end and digitization. This noise is highly uncorrelated: averaging over 750 pulses, to construct ECAP trace presentations, reduces noise on the recording cuff to 0.11 μV_{rms} compared to a theoretical reduction by $\sqrt{750}$ to 0.09 μV_{rms} if the noise was entirely uncorrelated (Metcalfe et al., 2018). Since most of the noise in this recording frequency band is coming from electronics front-end and digitization, application specific front-end and analog to digital converter (ADC) architecture and design can be exploited to reduce noise. Further tightening the recording bandwidth will also reduce RMS noise. Note that electronic noise may not be the dominant noise source in other recording frequency bands, such as local field potential (LFP) recordings.

For the higher impedance microneurography microelectrode, we see additional noise contributions for a total noise floor of 3.51 μV_{rms} on the microneurography microelectrode filtered time series trace versus 2.53 μV_{rms} on the lower impedance recording cuff trace. This difference of 0.98 μV_{rms} is likely attributable to electrode thermal noise and increased external noise, which is picked up by the longer length of the microneurography microelectrode. Note that while the impedance of the microneurography microelectrode used was specified to be 1 MOhm at 1 kHz, 1 MOhm would not be used as the resistance to calculate thermal noise as the

1 MOhm includes both real and imaginary impedance. Only real impedance (resistance) is used to calculate thermal noise. An ideal capacitor, despite having an imaginary impedance, does not generate thermal noise (Lundberg, 2002). Instead, the true thermal noise of the electrode is the noise calculated from the real impedance and filtered by the equivalent circuit capacitance of the electrode (Lundberg, 2002), and will be much lower than the 6.9 μV_{rms} calculated using 1 MOhm as the resistance (empirically there was only a 0.98 μV_{rms} noise floor increase on the much higher impedance microneurography microelectrode compared to the low impedance cuff).

Our recordings also showed that all three recording electrodes were susceptible to motion induced artifacts from respiration, cardiac activity, tremoring, etc. In this animal study, we were able to use controls such as nerve transections and administration of a muscle paralytic, vecuronium, to differentiate neural signals from artifact. However, use of these controls may not be feasible in a clinical setting. Therefore, one needs to be careful in interpreting clinical microneurography recordings that are expected to correlate to physiological events that also create motion, such as respiration, cardiac activity, etc. Inspection of neural spike shapes and control recordings from close-by non-neural tissue can help differentiate between neural signals and artifact and lend confidence to the reported neural recordings. High pass filtering to remove lower frequency artifact and placement of the reference electrode close to the recording electrode to lower common mode artifact can further reduce motion induced artifact in the recordings.

Correlation of VNS cardiac response and B-fiber ECAPs

A previous publication from our group showed strong tracking between Aα-fiber ECAP recordings and EMG activity recorded from the laryngeal muscles, implicated as off-target activation in clinical VNS for epilepsy (Blanz et al., 2022). However, the publication did not investigate tracking between stimulation-evoked decrease in heart rate and B-fiber ECAPs, which are putatively responsible for decreases in heart rate during VNS (Qing et al., 2018).

In Fig. 5, we show correlation between stimulation-evoked bradycardia and B-fiber ECAPs magnitude from a select subject. The trend was strong with cuff ECAP recordings (R_cuff = 0.70) but poor with intrafascicular recordings (R_LIFE = 0.39), which were the electrodes used exclusively in the previous study by our group (Blanz et al., 2022). Interestingly, shown in Fig. 5C, we saw an increasing response bradycardia till a VNS amplitude of ~5 mA, and then a decreased bradycardia response. We hypothesize that at higher stimulation currents, additional fiber types, which have a tachycardia effect, are activated, partially ‘cancelling out’ the bradycardia effect.

General limitations

A general limitation of our side-by-side characterization of recording electrode types for the peripheral nervous systems is the varying degree of surgical trauma created by the application of each electrode. The LIFE electrode insertion created the most trauma followed by the microneurography microelectrode, and lastly the cuff recording electrode. The open surgical preparation was not reflective of the minimally invasive clinical insertion typical with the microneurography electrode or the chronic healed-in recording state of an implanted cuff electrode. Another general limitation is that we did not fully optimize the design of each recording electrode type. However, there have been many studies that have used computational and *in vivo* methods to optimize the design of each recording electrode type (Yoshida and Stein, 1999; Boretius et al., 2010; Sabetian et al., 2017; Jiman et al., 2020; Ottaviani et al., 2020; Blanz et al., 2022). We drew from these studies and prior experience to inform the electrode design for each electrode type tested. Despite these limitations, we believe the strong effect sizes of the primary outcomes give validity to the study's conclusions.

Conclusions

This publication is the first to report on the side-by-side comparison of recording electrode types for recording electrically evoked compound action potentials (ECAPs) and sensory evoked neural activity in the peripheral nervous system of a human-scaled large animal model. We characterized a recording cuff, microneurography microelectrodes, and intrafascicular electrodes. We found that although the cuff records a significantly higher ECAP signal magnitude and has a lower noise floor than the microneurography microelectrode, the microneurography microelectrode may be the most sensitive recording electrode due to its proximity to the neural source. We compared 'local non-neural tissue' and 'on-nerve' bipolar and tripolar reference strategies that microneurography and cuff recordings lend themselves to naturally, respectively. We concluded that minimally invasive microneurography microelectrodes, already in routine human use, may be an important tool to develop and deploy neuromodulation therapies to attain greater specificity of local on-target neural engagement.

Acknowledgements

Dr. Jill Barnes for assistance with microneurography technique and electrode selection. Dr. Rick Chappell for insights and input on statistical design and analysis. Maria LaLuzerne for swine study scheduling and animal care. Jonah Mudge for fabricating electrodes used in the pilot experiments. Carly Frieders, Ashlesha Deshmukh, and Rex Chen for reviewing drafts of this manuscript. Members of the Wisconsin Institute for Translational Neuroengineering (WITNe) for feedback during group meetings.

This work was funded by the United States National Institute of Health (NIH) SPARC Program OT2OD025340.

Conflicts of Interest

NV is an employee of Abbott Neuromodulation and BioCircuit Technologies. KAL is a scientific board member and has stock interests in NeuroOne Medical Inc., a company developing next generation epilepsy monitoring devices. KAL is also a paid member of the scientific advisory board of Cala Health, Blackfynn, Abbott Neuromodulation, Presidio Medical, and Battelle. KAL also is a paid consultant for CVRx, Galvani, and the Alfred Mann Foundation. KAL is a co-founder of NeuronOff Inc.

The remaining authors declare that the research was conducted in the absence of any commercial or financial relationships that could be construed as a potential conflict of interest.

References

Ackerley, R., and Watkins, R. H. (2018). Microneurography as a tool to study the function of individual C-fiber afferents in humans: responses from nociceptors, thermoreceptors, and mechanoreceptors. *Journal of Neurophysiology* 120, 2834–2846. doi: 10.1152/jn.00109.2018.

Andreasen, L. N. S., and Struijk, J. J. (2002). Signal strength versus cuff length in nerve cuff electrode recordings. *IEEE Trans. Biomed. Eng.* 49, 1045–1050. doi: 10.1109/TBME.2002.800785.

Ardell, J. L., Nier, H., Hammer, M., Southerland, E. M., Ardell, C. L., Beaumont, E., et al. (2017). Defining the neural fulcrum for chronic vagus nerve stimulation: implications for integrated cardiac control: Vagus nerve stimulation neural fulcrum for cardiac control. *J Physiol* 595, 6887–6903. doi: 10.1113/JP274678.

Barry, J. M. (2015). Axonal activity in vivo: technical considerations and implications for the exploration of neural circuits in freely moving animals. *Front. Neurosci.* 9. doi: 10.3389/fnins.2015.00153.

Blanz, S. L., Musselman, E. D., Settell, M. L., Knudsen, B. E., Nicolai, E. N., Trevathan, J. K., et al. (2022). Spatially selective stimulation of the pig vagus nerve to modulate target effect versus side effect. Bioengineering doi: 10.1101/2022.05.19.492726.

Boretius, T., Badia, J., Pascual-Font, A., Schuettler, M., Navarro, X., Yoshida, K., et al. (2010). A transverse intrafascicular multichannel electrode (TIME) to interface with the peripheral nerve. *Biosensors and Bioelectronics* 26, 62–69. doi: 10.1016/j.bios.2010.05.010.

Bovik, A. C., and Acton, Scott T (2005). Basic Linear Filtering with Application to Image Enhancement. *Handbook of Image and Video Processing*, 10.

Buzsáki, G. (2004). Large-scale recording of neuronal ensembles. *Nat Neurosci* 7, 446–451. doi: 10.1038/nn1233.

Cakmak, Y. O., Apaydin, H., Kiziltan, G., Gündüz, A., Ozsoy, B., Olcer, S., et al. (2017). Rapid Alleviation of Parkinson's Disease Symptoms via Electrostimulation of Intrinsic Auricular Muscle Zones. *Front. Hum. Neurosci.* 11, 338. doi: 10.3389/fnhum.2017.00338.

Castoro, M. A. (2011). Excitation properties of the right cervical vagus nerve in adult dogs. *Experimental Neurology*, 7.

Chakravarthy, K., Bink, H., and Dinsmoor, D. (2020). Sensing Evoked Compound Action Potentials from the Spinal Cord: Novel Preclinical and Clinical Considerations for the Pain Management Researcher and Clinician. *JPR* Volume 13, 3269–3279. doi: 10.2147/JPR.S289098.

Chakravarthy, K., FitzGerald, J., Will, A., Trutnau, K., Corey, R., Dinsmoor, D., et al. (2022). A Clinical Feasibility Study of Spinal Evoked Compound Action Potential Estimation Methods. *Neuromodulation: Technology at the Neural Interface* 25, 75–84. doi: 10.1111/ner.13510.

Chao, D., Mecca, C. M., Yu, G., Segel, I., Gold, M. S., Hogan, Q. H., et al. (2021). Dorsal root ganglion stimulation of injured sensory neurons in rats rapidly eliminates their spontaneous activity and relieves spontaneous pain. *Pain* 162, 2917–2932. doi: 10.1097/j.pain.0000000000002284.

Chen, H. (1994). Comparisons of Lognormal Population Means. *Proceedings of the American Mathematical Society* 121, 915. doi: 10.2307/2160293.

De Ferrari, G. M., Stolen, C., Tuinenburg, A. E., Wright, D. J., Brugada, J., Butter, C., et al. (2017). Long-term vagal stimulation for heart failure: Eighteen month results from the NEural Cardiac TherApy foR Heart Failure (NECTAR-HF) trial. *International Journal of Cardiology* 244, 229–234. doi: 10.1016/j.ijcard.2017.06.036.

Donaldson, N., Rieger, R., Schuettler, M., and Taylor, J. (2008). Noise and selectivity of velocity-selective multi-electrode nerve cuffs. *Med Biol Eng Comput* 46, 1005–1018. doi: 10.1007/s11517-008-0365-4.

Drebitz, E. (2020). A novel approach for removing micro-stimulation artifacts and reconstruction of broad-band neuronal signals. *Journal of Neuroscience Methods*, 11.

Duisit, J., Debluts, D., Behets, C., Gerdom, A., Vlassenbroek, A., Coche, E., et al. (2017). Porcine ear: A new model in large animals for the study of facial subunit allotransplantation. *JPRAS Open* 12, 47–58. doi: 10.1016/j.jpra.2017.01.004.

Erlanger, J., and Gasser, H. (1937). Electrical Signs of Nervous Activity (London: University of Pennsylvania Press)

Feucht, M., Ward, M. (2021). Non-invasive, Spatiotemporal Characterization of Muscle Activation Patterns from Vagus Nerve Stimulation in Human Subjects, DOI: https://doi.org/10.18060/25920

Gaunt, R. A., Hokanson, J. A., and Weber, D. J. (2009). Microstimulation of primary afferent neurons in the L7 dorsal root ganglia using multielectrode arrays in anesthetized cats: thresholds and recruitment properties. *J. Neural Eng.* 6, 055009. doi: 10.1088/1741-2560/6/5/055009.

Getty, R., and Grossman, J. D. (1975). The Anatomy of the Domestic Animals, Vol. 2 ISBN: 0721641075, W B Saunders Co.

Gonzalez-Gonzalez, M. A., Bendale, G. S., Wang, K., Wallace, G. G., and Romero-Ortega, M. (2021). Platinized graphene fiber electrodes uncover direct spleen-vagus communication. *Commun Biol* 4, 1097. doi: 10.1038/s42003-021-02628-7.

Harding, G. W. (1991). A method for eliminating the stimulus artifact from digital recordings of the direct cortical response. *Computers and Biomedical Research* 24, 183–195. doi: 10.1016/0010-4809(91)90029-V.

He, S., Teagle, H. F. B., and Buchman, C. A. (2017). The Electrically Evoked Compound Action Potential: From Laboratory to Clinic. *Front. Neurosci.* 11, 339. doi: 10.3389/fnins.2017.00339.

Heusser, K., Tank, J., Brinkmann, J., Menne, J., Kaufeld, J., Linnenweber-Held, S., et al. (2016). Acute Response to Unilateral Unipolar Electrical Carotid Sinus Stimulation in Patients With Resistant Arterial Hypertension. *Hypertension* 67, 585–591. doi: 10.1161/HYPERTENSIONAHA.115.06486.

Humphrey, Donald, and Schmidt, Edward (1990). *Neurophysiological Techniques*.

Janko, M., and Trontelj, J. V. (1980). TRANSCUTANEOUS ELECTRICAL NERVE STIMULATION: A MICRONEUROGRAPHIC AND PERCEPTUAL STUDY. 12.

Jiman, A. A., Ratze, D. C., Welle, E. J., Patel, P. R., Richie, J. M., Bottorff, E. C., et al. (2020). Multi-channel intraneural vagus nerve recordings with a novel high-density carbon fiber microelectrode array. *Sci Rep* 10, 15501. doi: 10.1038/s41598-020-72512-7.

Johnson, R. L., and Wilson, C. G. (2018). A review of vagus nerve stimulation as a therapeutic intervention. *JIR* Volume 11, 203–213. doi: 10.2147/JIR.S163248.

Kaniusas, E., Kampusch, S., Tittgemeyer, M., Panetsos, F., Gines, R. F., Papa, M., et al. (2019). Current Directions in the Auricular Vagus Nerve Stimulation I – A Physiological Perspective. *Front. Neurosci.* 13, 854. doi: 10.3389/fnins.2019.00854.

Khodagholy, D., Gelinas, J. N., Thesen, T., Doyle, W., Devinsky, O., Malliaras, G. G., et al. (2015). NeuroGrid: recording action potentials from the surface of the brain. *Nat Neurosci* 18, 310–315. doi: 10.1038/nn.3905.

Kodandaramaiah, S. B., Franzesi, G. T., Chow, B. Y., Boyden, E. S., and Forest, C. R. (2012). Automated whole-cell patch-clamp electrophysiology of neurons in vivo. *Nat Methods* 9, 585–587. doi: 10.1038/nmeth.1993.

Koh, R. G. L., Zariffa, J., Jabban, L., Yen, S.-C., Donaldson, N., and Metcalfe, B. W. (2022). Tutorial: A guide to techniques for analysing recordings from the peripheral nervous system. *J. Neural Eng.* doi: 10.1088/1741-2552/ac7d74.

Koppaka, S., Hess-Dunning, A., and Tyler, D. J. (2022). Biomechanical characterization of isolated epineurial and perineurial membranes of rabbit sciatic nerve. *Journal of Biomechanics* 136, 111058. doi: 10.1016/j.jbiomech.2022.111058.

Lefkowitz, T., Hazani, R., Chowdhry, S., Elston, J., Yaremchuk, M. J., and Wilhelmi, B. J. (2013). Anatomical Landmarks to Avoid Injury to the Great Auricular Nerve During Rhytidectomy. *Aesthetic Surgery Journal* 33, 19–23. doi: 10.1177/1090820X12469625.

Lundberg, K. H. Noise Sources in Bulk CMOS. 12.

Macefield, V. G. (2021). Recording and quantifying sympathetic outflow to muscle and skin in humans: methods, caveats and challenges. *Clin Auton Res* 31, 59–75. doi: 10.1007/s10286-020-00700-6.

Manzano, G. M., Giuliano, L. M. P., and Nóbrega, J. A. M. (2008). A brief historical note on the classification of nerve fibers. *Arq. Neuro-Psiquiatr.* 66, 117–119. doi: 10.1590/S0004-282X2008000100033.

Meier, K., Qerama, E., Ettrup, K. S., Glud, A. N., Alstrup, A. K. O., and Sørensen, J. C. H. (2018). Segmental innervation of the Göttingen minipig hind body. An electrophysiological study. *J. Anat.* 233, 411–420. doi: 10.1111/joa.12865.

Mekhail, N., Levy, R. M., Deer, T. R., Kapural, L., Li, S., Amirdelfan, K., et al. (2022). Durability of Clinical and Quality-of-Life Outcomes of Closed-Loop Spinal Cord Stimulation for Chronic Back

and Leg Pain: A Secondary Analysis of the Evoke Randomized Clinical Trial. *JAMA Neurol* 79, 251. doi: 10.1001/jamaneurol.2021.4998.

Metcalfe, B. W., Nielsen, T. N., Donaldson, N. de N., Hunter, A. J., and Taylor, J. T. (2018). First demonstration of velocity selective recording from the pig vagus using a nerve cuff shows respiration afferents. *Biomed. Eng. Lett.* 8, 127–136. doi: 10.1007/s13534-017-0054-z.

Mitra, S., Mitra, M., and Halder, B. (2018). Automatic feature extraction of ECG signal based on adaptive window dependent differential histogram approach and validation with CSE database. *IJCSYSE* 4, 146. doi: 10.1504/IJCSYSE.2018.10012644.

Molecular Devices. (2006). The Axon CNS Guide. pg 235-263 Part Number 2500-102 Rev B 200

Moncrief, K., and Kaufman, S. (2006). Splenic baroreceptors control splenic afferent nerve activity. *American Journal of Physiology-Regulatory, Integrative and Comparative Physiology* 290, R352–R356. doi: 10.1152/ajpregu.00489.2005.

Nicolai, E. N., Settell, M. L., Knudsen, B. E., McConico, A. L., Gosink, B. A., Trevathan, J. K., et al. (2020). Sources of off-target effects of vagus nerve stimulation using the helical clinical lead in domestic pigs. *J. Neural Eng.* 17, 046017. doi: 10.1088/1741-2552/ab9db8.

Nonis, R., D'Ostilio, K., Schoenen, J., and Magis, D. (2017). Evidence of activation of vagal afferents by non-invasive vagus nerve stimulation: An electrophysiological study in healthy volunteers. *Cephalalgia* 37, 1285–1293. doi: 10.1177/0333102417717470.

Obot, I. B., Onyeachu, I. B., Zeino, A., and Umoren, S. A. (2019). Electrochemical noise (EN) technique: review of recent practical applications to corrosion electrochemistry research. *Journal of Adhesion Science and Technology* 33, 1453–1496. doi: 10.1080/01694243.2019.1587224.

Ottaviani, M. M., Wright, L., Dawood, T., and Macefield, V. G. (2020). In vivo recordings from the human vagus nerve using ultrasound-guided microneurography. *J Physiol*, JP280077. doi: 10.1113/JP280077.

Park, J., Choi, W.-M., Kim, K., Jeong, W.-I., Seo, J.-B., and Park, I. (2018). Biopsy Needle Integrated with Electrical Impedance Sensing Microelectrode Array towards Real-time Needle Guidance and Tissue Discrimination. *Sci Rep* 8, 264. doi: 10.1038/s41598-017-18360-4.

Parker, J. L., Karantonis, D. M., Single, P. S., Obradovic, M., and Cousins, M. J. (2012). Compound action potentials recorded in the human spinal cord during neurostimulation for pain relief. *Pain* 153, 593–601. doi: 10.1016/j.pain.2011.11.023.

Parker, J. L., Obradovic, M., Hesam Shariati, N., Gorman, R. B., Karantonis, D. M., Single, P. S., et al. (2020). Evoked Compound Action Potentials Reveal Spinal Cord Dorsal Column Neuroanatomy. *Neuromodulation: Technology at the Neural Interface* 23, 82–95. doi: 10.1111/ner.12968.

Qing, K. Y., Wasilczuk, K. M., Ward, M. P., Phillips, E. H., Vlachos, P. P., Goergen, C. J., et al. (2018). B fibers are the best predictors of cardiac activity during Vagus nerve stimulation: Qing, vagal B fiber activation and cardiac effects. *Bioelectron Med* 4, 5. doi: 10.1186/s42234-018-0005-8.

Rawlins, J. C. (2000). "AC and the Sine Wave," in *Basic AC Circuits* (Elsevier), 29–63. doi: 10.1016/B978-075067173-6/50003-1.

Ringer, S. K., Spielmann, N., Weiss, M., and Mauch, J. Y. (2016). Fentanyl bolus induces muscle tremors in sevoflurane-anaesthetized piglets. *Lab Anim* 50, 312–314. doi: 10.1177/0023677215623896.

Robinson, D. A. (1968). The electrical properties of metal microelectrodes. *Proc. IEEE* 56, 1065–1071. doi: 10.1109/PROC.1968.6458.

Sabbah, H. N., Ilsar, I., Zaretsky, A., Rastogi, S., Wang, M., and Gupta, R. C. (2011). Vagus nerve stimulation in experimental heart failure. *Heart Fail Rev* 16, 171–178. doi: 10.1007/s10741-010-9209-z.

Sabetian, P., Popovic, M. R., and Yoo, P. B. (2017). Optimizing the design of bipolar nerve cuff electrodes for improved recording of peripheral nerve activity. *J. Neural Eng.* 14, 036015. doi: 10.1088/1741-2552/aa6407.

Scipy. (2022). scipy.signal.filtfilt accessed at https://docs.scipy.org/doc/scipy/reference/generated/scipy.signal.filtfilt.html

Settell, M. L., Pelot, N. A., Knudsen, B. E., Dingle, A. M., McConico, A. L., Nicolai, E. N., et al. (2020). Functional vagotopy in the cervical vagus nerve of the domestic pig: implications for the study of vagus nerve stimulation. *J. Neural Eng.* 17, 026022. doi: 10.1088/1741-2552/ab7ad4.

Sharma, V. S., Stephens, R. E., Wright, B. W., and Surek, C. C. (2017). What Is the Lobular Branch of the Great Auricular Nerve? Anatomical Description and Significance in Rhytidectomy: *Plastic and Reconstructive Surgery* 139, 371e–378e. doi: 10.1097/PRS.0000000000002980.

Silverman, H. A., Stiegler, A., Tsaava, T., Newman, J., Steinberg, B. E., Masi, E. B., et al. (2018). Standardization of methods to record Vagus nerve activity in mice. *Bioelectron Med* 4, 3. doi: 10.1186/s42234-018-0002-y.

Simakov, A. B., and Webster, J. G. (2010). MOTION ARTIFACT FROM ELECTRODES AND CABLES. 9, 5.

Stumpp, L., Smets, H., Vespa, S., Cury, J., Doguet, P., Delbeke, J., et al. (2020). Recording of spontaneous vagus nerve activity during Pentylenetetrazol-induced seizures in rats. *Journal of Neuroscience Methods* 343, 108832. doi: 10.1016/j.jneumeth.2020.108832.

Tucker-Davis Technologies, Inc. (TDT). (2022). SIM Subject Interface Module Hardware Reference, Page 23

Ulrich, G., Schlosser, W., and Juckel, G. (2016). The impact of Arterial Pulse Impedance Artifact (APIA) on test-retest reliability of quantitative EEG. *Neuropsychiatr Electrophysiol* 2, 5. doi: 10.1186/s40810-016-0019-y.

Verma, N., Graham, R. D., Mudge, J., Trevathan, J. K., Franke, M., Shoffstall, A. J., et al. (2021a). Augmented Transcutaneous Stimulation Using an Injectable Electrode: A Computational Study. *Front. Bioeng. Biotechnol.* 9, 796042. doi: 10.3389/fbioe.2021.796042.

Verma, N., Mudge, J. D., Kasole, M., Chen, R. C., Blanz, S. L., Trevathan, J. K., et al. (2021b). Auricular Vagus Neuromodulation—A Systematic Review on Quality of Evidence and Clinical Effects. *Front. Neurosci.* 15, 664740. doi: 10.3389/fnins.2021.664740.

Winestone, J. S., Zaidel, A., Bergman, H., and Israel, Z. (2012). The use of macroelectrodes in recording cellular spiking activity. *Journal of Neuroscience Methods* 206, 34–39. doi: 10.1016/j.jneumeth.2012.02.002.

Yang, H.-M., Kim, H.-J., and Hu, K.-S. (2015). Anatomic and histological study of great auricular nerve and its clinical implication. *Journal of Plastic, Reconstructive & Aesthetic Surgery* 68, 230–236. doi: 10.1016/j.bjps.2014.10.030.

Yang, Z., Zhao, Q., Keefer, E., and Liu, W. Noise Characterization, Modeling, and Reduction for In Vivo Neural Recording. 9.

Yasar, N. (2021) Causes of noise in electrophysiological recordings. *Plexon blog*. accessed at https://plexon.com/blog-post/causes-of-noise-in-electrophysiological-recordings/

Yoo, P. B., Lubock, N. B., Hincapie, J. G., Ruble, S. B., Hamann, J. J., and Grill, W. M. (2013). High-resolution measurement of electrically-evoked vagus nerve activity in the anesthetized dog. *J. Neural Eng.* 10, 026003. doi: 10.1088/1741-2560/10/2/026003.

Yoshida, K., and Stein, R. B. (1999). Characterization of signals and noise rejection with bipolar longitudinal intrafascicular electrodes. *IEEE Trans. Biomed. Eng.* 46, 226–234. doi: 10.1109/10.740885.